Supporting Information

Pyridine-Chelated Imidazo[1,5-a]pyridine *N*-Heterocyclic Carbene Nickel(II) Complexes for Acrylate Synthesis from Ethylene and CO_2

Jiyun Kim[1], Hyungwoo Hahm[1], Ji Yeon Ryu[2], Seunghwan Byun,[1] Da-Ae Park,[1] Seoung Ho Lee,[3] Hyunseob Lim,[1] Junseong Lee[2], and Sukwon Hong[1,4*]

[1]Department of Chemistry, Gwangju Institute of Science and Technology, 123 Chemdan-gwagiro, Buk-gu, Gwangju 61005, Republic of Korea

[2]Department of Chemistry, Chonnam National University, 77 Yongbongro, Buk-gu, Gwangju 61186, Republic of Korea

[3]Department of Chemistry, Institute of Basic Sciences, Daegu University, Gyeongsan 38453, Republic of Korea

[4]School of Materials Science and Engineering, Gwangju Institute of Science and Technology, 123 Chemdan-gwagiro, Buk-gu, Gwangju 61005, Republic of Korea

Table of Contents

General remarks

All air- and moisture-sensitive reactions were performed under an argon atmosphere either using Schlenk techniques or a glove box. All reactions involving the formation of acrylate from ethylene and CO_2 were carried out in 100-mL stainless steel autoclaves. Nuclear magnetic resonance (NMR) spectra were recorded on a JEOL 400 spectrometer, operated at 400 MHz for ^{1}H NMR and at 100 MHz for ^{13}C NMR. Chemical shifts (ppm) for ^{1}H were referenced to the residual solvent peak ($CDCl_3$ = δ 7.26 ppm, CD_2Cl_2 = δ 5.32 ppm, CD_3OD = δ 3.31 ppm, $(CD_3)_2SO$= 2.50 ppm, D_2O = δ 4.79 ppm). Multiplicities were recorded as s (singlet), d (doublet), t (triplet), q (quartet), sept (septet), or m (multiplet). Chemical shifts (ppm) for ^{13}C were referenced relative to the residual solvent peak (CD_2Cl_2 = δ 53.84 ppm, CD_3OD = δ 49.00 ppm, $(CD_3)_2SO$= 39.52 ppm). High-resolution mass spectra (HRMS) were recorded on a JEOL JMS-700 MStation mass spectrometer. Elemental analyses were carried out with an UNICUBE Elemental Analyzer. The magnetic susceptibilities of nickel complexes were measured in the solid state using a magnetic susceptibility balance (Sherwood Scientific, Cambridge, UK). Diamagnetic corrections were ignored. UV/vis measurements of nickel complexes were carried out in CH_2Cl_2 solution using a Perkin-Elmer UV/VIS NIR Spectrometer Lambda 950. Analytical thin layer chromatography (TLC) was performed with Merck pre-coated silica gel 60 Å (F254) glass plates and visualization on TLC was achieved by UV light. Flash chromatography was performed with 230–400 Mesh 60 Å Silica Gel purchased from Merck Inc.

Materials: Ethylene gas (99.999%) and carbon dioxide (99.99%) were purchased from Sinil Gas Co. Ethylene was purified by passing through a column packed with BASF catalyst R3-11G, activated carbon and 4 Å molecular sieves. Carbon dioxide was dried by passing through a column packed with 4 Å molecular sieves. All the chemicals were purchased from Aldrich,

Acros, TCI, or Alfa-Aesar Chemical Co. and used as received unless otherwise noted. Anhydrous tetrahydrofuran (THF), diethyl ether (Et_2O), dichloromethane (CH_2Cl_2) and dimethylformamide (DMF) were dried using a J.C. Meyer solvent purification system. Triethyl amine, toluene and hexane were distilled from calcium hydride. Methanol and ethanol were dried over 4 Å molecular sieves.

Scheme S1: *in-situ* nickel(II) mediated C-H carboxylation of ethylene using CO_2[a]

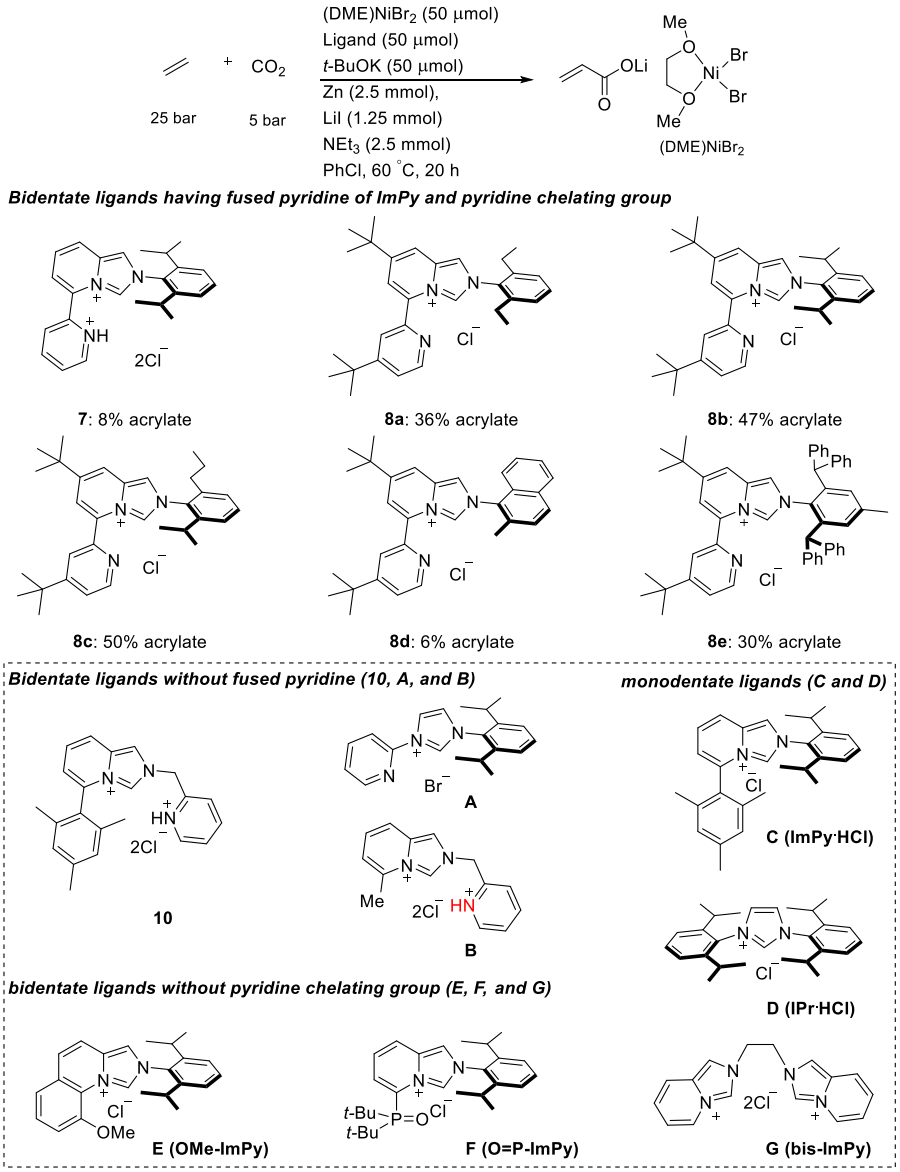

[a] % acrylate determined by ^{1}H NMR spectroscopy using lithium acetate dehydrate or sodium 3-(trimethylsilyl)-2,2,3,3-d$_4$-propionate as the internal standard. % acrylate = (mmol acrylate)/(mmol Ni) × 100; ligand precursors including 2 equiv. of HCl: 100 μmol *t*-BuOK.

Note: In the dashed box, the ligand precursors (**10** and **A-H**) did not show measurable activities in acrylate synthesis. The activities were only observed for the ImPy ligands bearing the pyridine chelating group at the C(5) position.

Scheme S2. Screening of monodentate phosphine additives in acrylate synthesis using ethylene and CO_2[a]

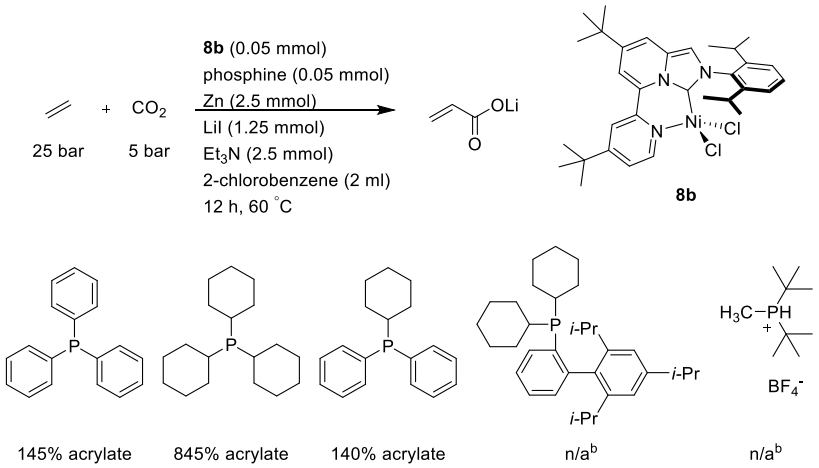

[a] % acrylate determined by ^{1}H NMR spectroscopy using sodium 3-(trimethylsilyl)-2,2,3,3-d_4-propionate as the internal standard. % acrylate = (mmol acrylate)/(mmol Ni) × 100 [b] Signals related to acrylate could not be reliably measured during the integration.

Scheme S3: Screening of bisphosphine ligands in acrylate synthesis using ethylene and CO_2[a]

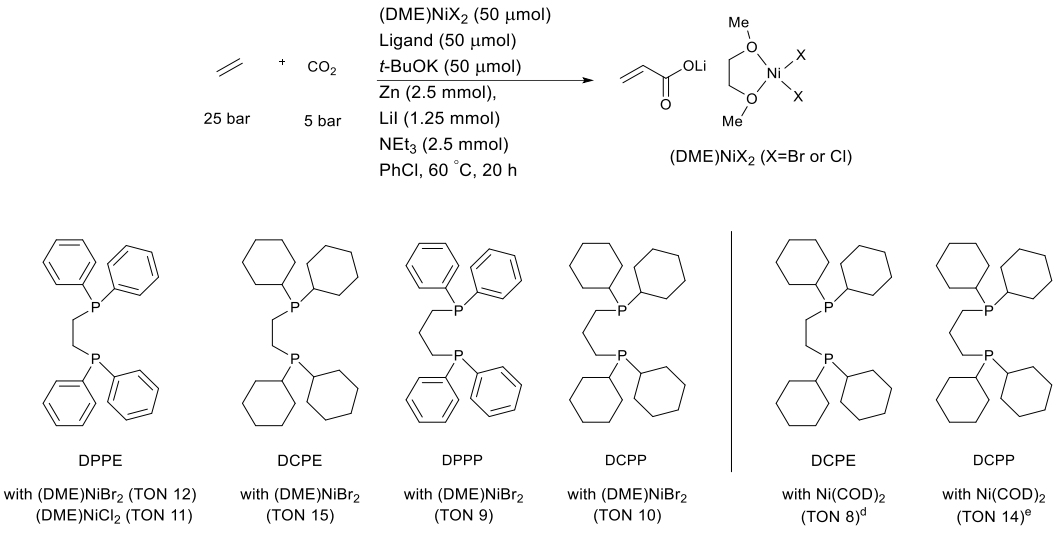

[a] Reaction conditions: 50 μmol Ni(II), 50 μmol ligand, 1.25 mmol LiI, 2.5 mmol Et_3N, 2 mL chlorobenzene, 2.5 mmol Zn, 20 h, 60°C. [b] Determined by ^1H NMR spectroscopy with an internal standard ($LiOAc.2H_2O$). [c] Signals related to acrylate could not be reliably measured during the integration. [d] reference [1]: 50 °C, 24 h [e] reference [2]: 50 °C, 72 h

Scheme S4: Screening of bidentate N-N ligands in acrylate synthesis using ethylene and CO_2[a]

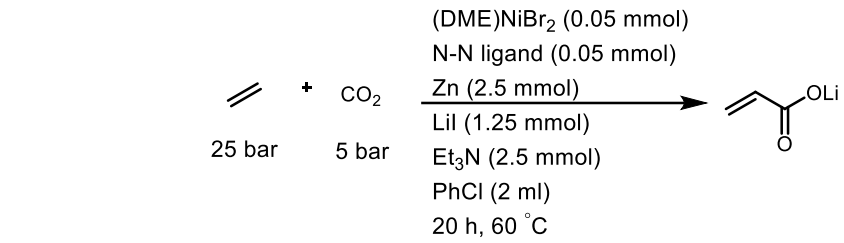

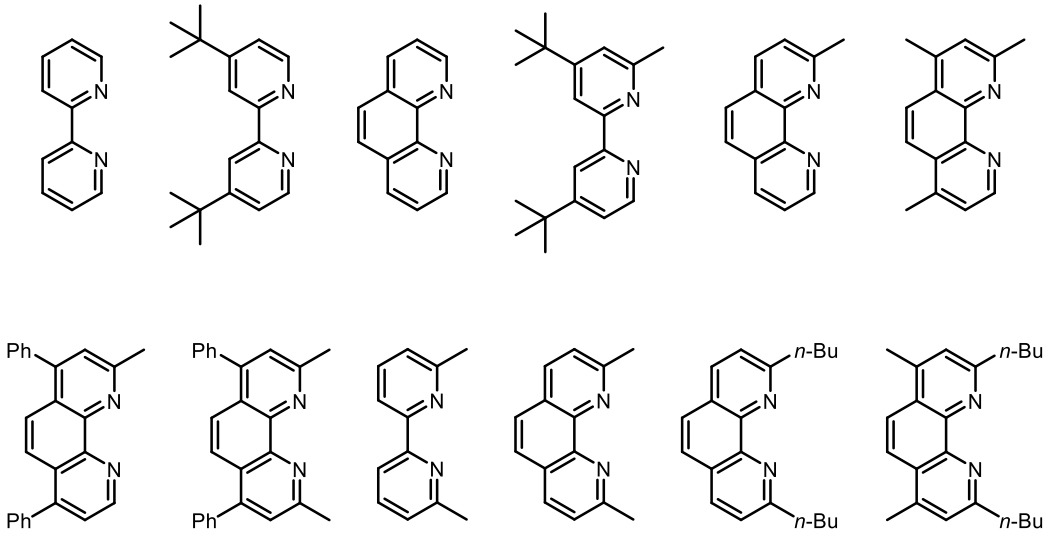

[a] % acrylate determined by ^{1}H NMR spectroscopy using lithium acetate dehydrate as the internal standard. % acrylate = (mmol acrylate)/(mmol Ni) × 100

Note: The above-mentioned bidentate N-N ligands showed no reactivity during acrylate synthesis using ethylene and CO_2.

4,4'-di-*tert*-butyl-[2,2'-bipyridine]-6-carbaldehyde (2).

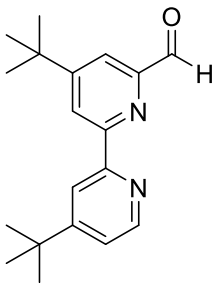

In a 100 mL Schlenk flask equipped with a Teflon-valve, 4,4'-di-*tert*-butyl-6-methyl-2,2'-bipyridine (1.60 g, 5.66 mmol), dioxane (56 mL), selenium dioxide (2.51 g, 22.6 mmol), and DI water (0.6 mL) were vigorously stirred at 120 °C for 48 h. The mixture was subsequently filtered through Celite and the solvent was removed by rotary evaporation. The crude was extracted with dichloromethane and then purified via flash column chromatography (From hexane:ethyl acetate = 15: 1) to yield an ivory solid **1b** (995 mg, 60% yield). ^{1}H NMR (400 MHz, CD_2Cl_2) δ 10.19 (s, 1H), 8.71 (d, J = 1.9 Hz, 1H), 8.61 – 8.59 (m, 2H), 7.99 (d, J = 1.9 Hz, 1H), 7.38 – 7.36 (m, 1H), 1.41 (s, 18H). ^{13}C NMR (100 MHz, CD_2Cl_2) δ 194.50, 162.80, 161.57, 157.45, 155.62, 152.94, 149.51, 122.66, 121.72, 118.70, 118.55, 35.65, 35.32, 30.74, 30.71. HR-MS (EI): calcd. for $C_{19}H_{24}N_2O$ [M] 296.1889 found 296.1886. Elemental analysis [%] Calcd. for $C_{19}H_{24}N_2O$: C, 76.99; H, 8.16; N, 9.45. Found: C, 76.98; H, 8.363; N, 9.35.

Preparation of ligands used in *in-situ* formation of catalysts (Scheme S1)

Ligand precursors **A** [3], **C** [4], **D** [5], **F** [6], and **G** [7] were synthesized according to the reported literature.

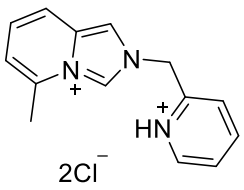

5-methyl-2-(pyridin-1-ium-2-ylmethyl)-2H-imidazo[1,5-a]pyridiniu-m dichloride (B, Scheme S1). The preparation of a product **B** from 6-methylpicolinaldehyde (4.40 mmol) is the same as that of **10**. The crude mixture was purified by silica column chromatography (CH_2Cl_2:MeOH=8:1). Recrystallization from MeOH/MC/ether afforded an ivory powder (865 mg, 66% yield). ^{1}H NMR (400 MHz, CD_3OD) δ 10.05 (s, 1 H), 8.96 (d, J = 5.7 Hz, 1 H), 8.67 (t, J = 7.9 Hz, 1 H), 8.41 (s, 1 H), 8.16-8.11 (m, 2 H), 7.79 (d, J = 9.4 Hz, 1 H), 7.34 (t, J = 6.9 Hz, 1 H), 7.13 (d, J = 6.9 Hz, 1 H), 6.38 (s, 2 H), 2.79 (s, 3 H). ^{13}C NMR (100 MHz, CD_3OD) δ 149.6, 148.5, 144.3, 134.7, 132.9, 128.4, 128.1, 127.3, 127.2, 118.3, 117.1, 115.5, 51.7, 18.0 HR-MS (FAB): calcd. for $C_{14}H_{14}N_3$ [M-H-2Cl]$^+$ 224.1182 found 224.1199. Calcd. for $C_{14}H_{15}Cl_2N_3$: C, 56.77; H, 5.10; N, 14.19. Found: C, 56.45; H, 5.412; N, 14.2.

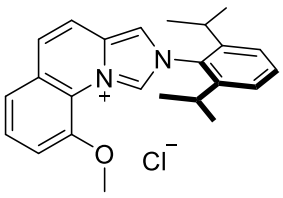

2-(2,6-diisopropylphenyl)-9-methoxy-2H-imidazo[1,5-a]quinol-inium chloride (E, Scheme S1). 8-methoxyquinoline-2-carbaldehyde was synthesized according to the reported method [8]. A product **E** was prepared following the general procedure of ligand precursors. 8-methoxyquinoline-2-carbaldehyde (206 mg, 1.10 mmol), 2,6-diisopropylaniline (207㎕, 1.1 mmol) and ethanol (3.4 mL) were refluxed for 24 h. After purification by basic silica gel column chromatography (hexane: EA = 6:1), the generated yellow solid was reacted with chloromethyl ethyl ether (2 mL, 22.0 mmol) at 100 ℃ for 20 h. The crude mixture was purified by silica gel column

chromatography (CH_2Cl_2:MeOH=8:1) and recrystallization (CH_2Cl_2/hexane) to yield product (white solid, 434 mg, quant.) ^{1}H NMR (400 MHz, CD_3OD) δ 10.67 (d, J = 1.6 Hz, 1H), 8.40 (d, J = 1.7 Hz, 1H), 7.79 – 7.73 (m, 3H), 7.71 – 7.66 (m, 1H), 7.60 (ddd, J = 15.7, 8.1, 1.0 Hz, 2H), 7.52 (d, J = 7.8 Hz, 2H), 4.20 (s, 3H), 2.34 (sept, J = 6.8 Hz, 2H), 1.25 (dd, J = 11.5, 6.8 Hz, 12H). ^{13}C NMR (101 MHz, CD_3OD) δ 150.95, 145.50, 132.75, 131.75, 131.39, 130.37, 129.38, 127.80, 127.21, 124.46, 121.18, 119.80, 116.88, 115.08, 112.41, 56.13, 28.57, 23.31, 22.96. HR-MS (FAB): calcd. for $C_{24}H_{27}N_2O$ $[M\text{-}Cl]^+$ 359.2117 found 359.2110.

Percent buried volume (*%V*$_{bur}$) of Ni(II) complexes

To compare steric environments around the metal center in detail, the percent buried volume (*%V*$_{bur}$) was calculated using SambVca [9]. Figure S1 shows the steric maps and *%V*$_{bur}$ values generated for Ni(II) complexes (**7, 8b, and 12**). As expected, *tert*-butyl substituents on the ligand backbone did not significantly affect the steric hindrance around the metal center. The Ni(II) complexes (**7, 8b, and 12**) have larger %VBur than that of the Ni(II) complex (**7, 8b, and 12**). These results show that substituents at C(5) on ImPy ligands have a significant impact on the Ni center.

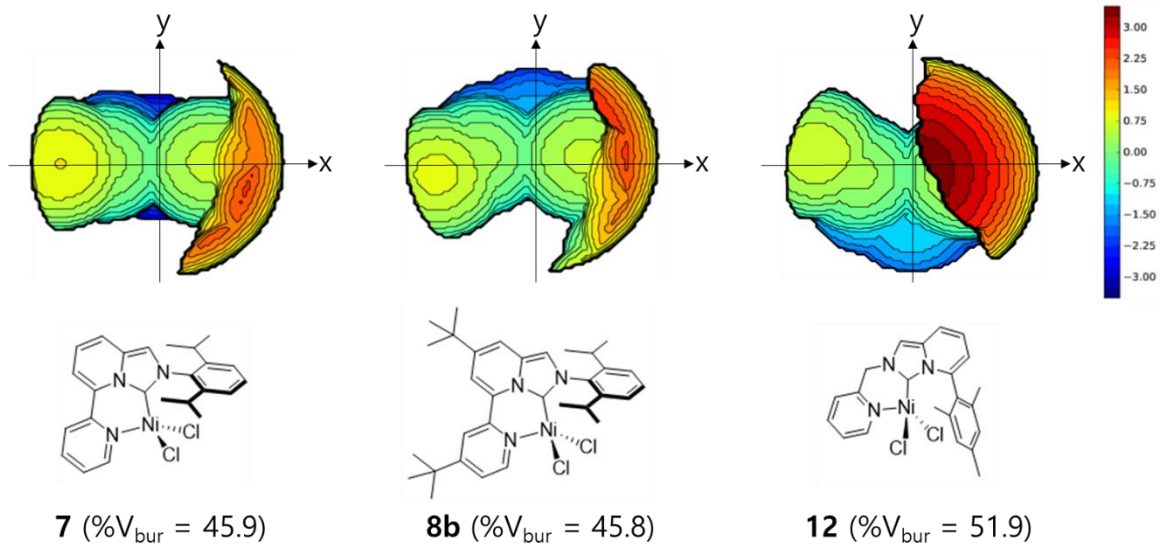

Figure S1. Steric maps of complexes (**7**, **8b**, and **12)** generated using the software SambVca 2.0 (sphere radius of 3.5 Å, 0.10 Å mesh spacing, Bond radii scaled by 1.17, Ni in the center of the sphere, H atoms omitted).

General procedure for the synthesis of lithium acrylate using ethylene and CO_2

In a glove box, a 4 mL screw-cap vial containing a stirring bar was charged with (DME)$NiBr_2$ (0.05 mmol), ligand precursors (0.05 mmol), and *t*-BuOK (0.05 mmol). The vial was sealed and removed from the glove box. The solid mixture was dissolved in chlorobenzene (2 mL), and then stirred for 15 min under argon atmosphere and at room temperature. The vial was then put into the glove box and LiI (1.25 mmol) and Zn (2.50 mmol) were added. Subsequently, the vial was capped and removed from the glove box. After stirring for 3 min, Et_3N (0.35 mL) was added via a syringe. Under argon atmosphere, the vial was transferred to a 100 mL stainless steel autoclave and was punctured with a flat-cut needle (18 G, 0.6 cm). The autoclave was immediately closed and purged with ethylene gas (10 bar) for 10 min without stirring. The autoclave was pressurized with ethylene (25 bar) and then with CO_2 (5 bar) at room temperature. The autoclave was heated to 60 ℃ in an oil bath for 12 h. After cooling to room temperature, the pressure was released. D_2O (1 mL) with sodium 3-(trimethylsilyl)-2,2,3,3-d_4-propionate (0.070 mmol), was added to the reaction mixture as an internal standard. After vigorous stirring for 15 min and manual shaking for about 15 min, the D_2O layer was separated from organic phase by centrifugation and filtration. The D_2O layer was washed with ether (2 mL). The amount of acrylate was determined by ^1H NMR of the D_2O layer.

If the internal standard is LiOAc•$2H_2O$, it is calculated as follows:

$$\%\ \text{acrylate} = \frac{\text{the total area of the acrylate signals}}{\text{the methyl signal of the LiOAc}\cdot 2H_2O\ \text{(Internal standard)}} \times \frac{\text{mmol LiOAc}\cdot 2H_2O}{\text{mmol Ni}} \times 100$$

$$\text{TON} = \frac{\text{the total area of the acrylate signals}}{\text{the methyl signal of the LiOAc}\cdot 2H_2O\ \text{(Internal standard)}} \times \frac{\text{mmol LiOAc}\cdot 2H_2O}{\text{mmol Ni}}$$

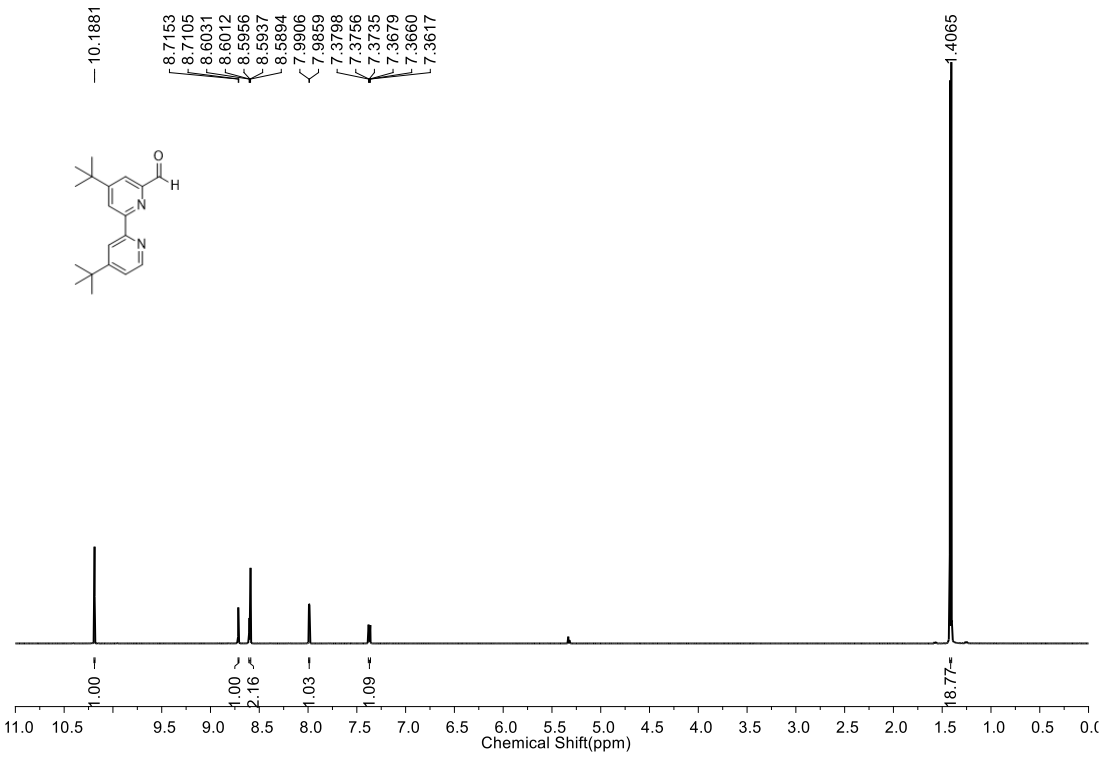

Figure S2 ^{1}H NMR spectrum of **2** in CD_2Cl_2 at 25 ℃

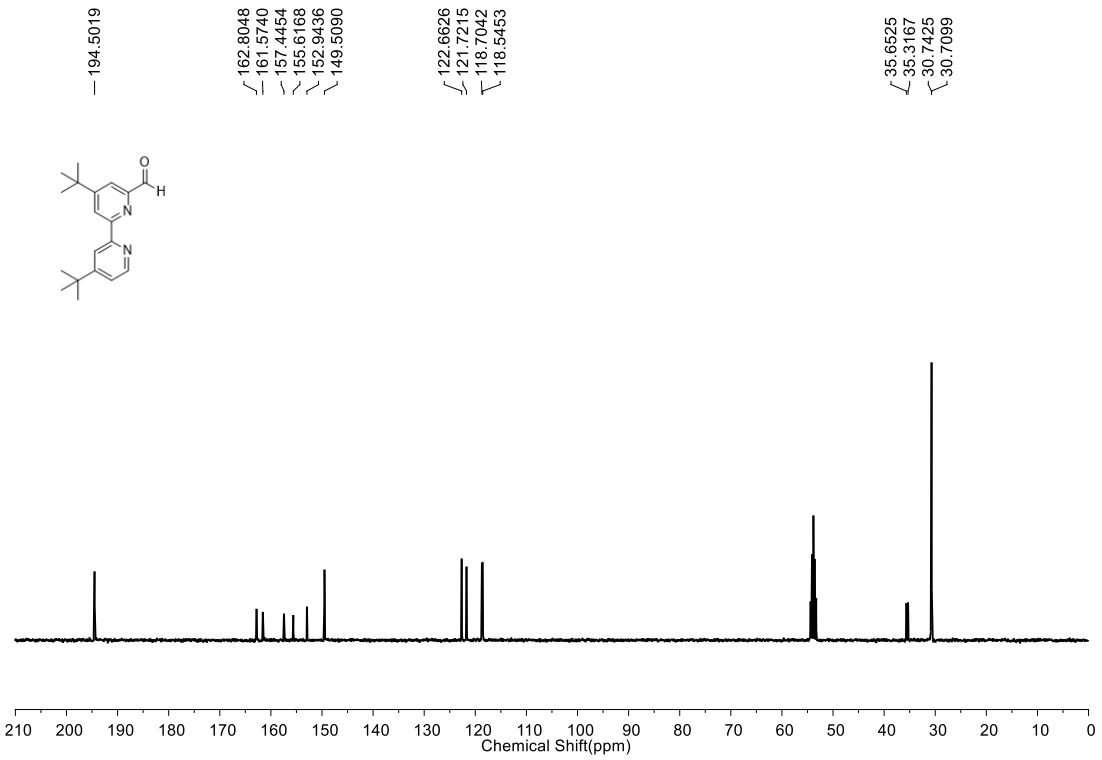

Figure S3 ^{13}C{^{1}H}NMR spectrum of **2** in CD_2Cl_2 at 25 ℃

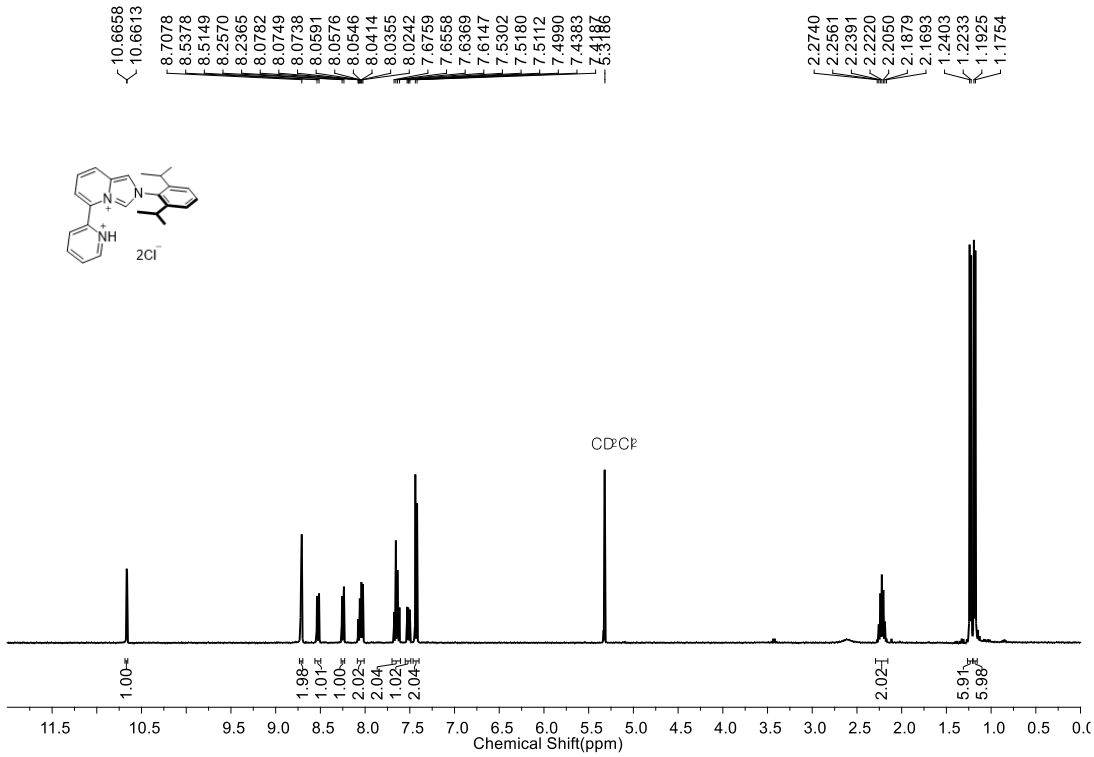

Figure S4 ^{1}H NMR spectrum of **3** in CD_2Cl_2 at 25 ℃

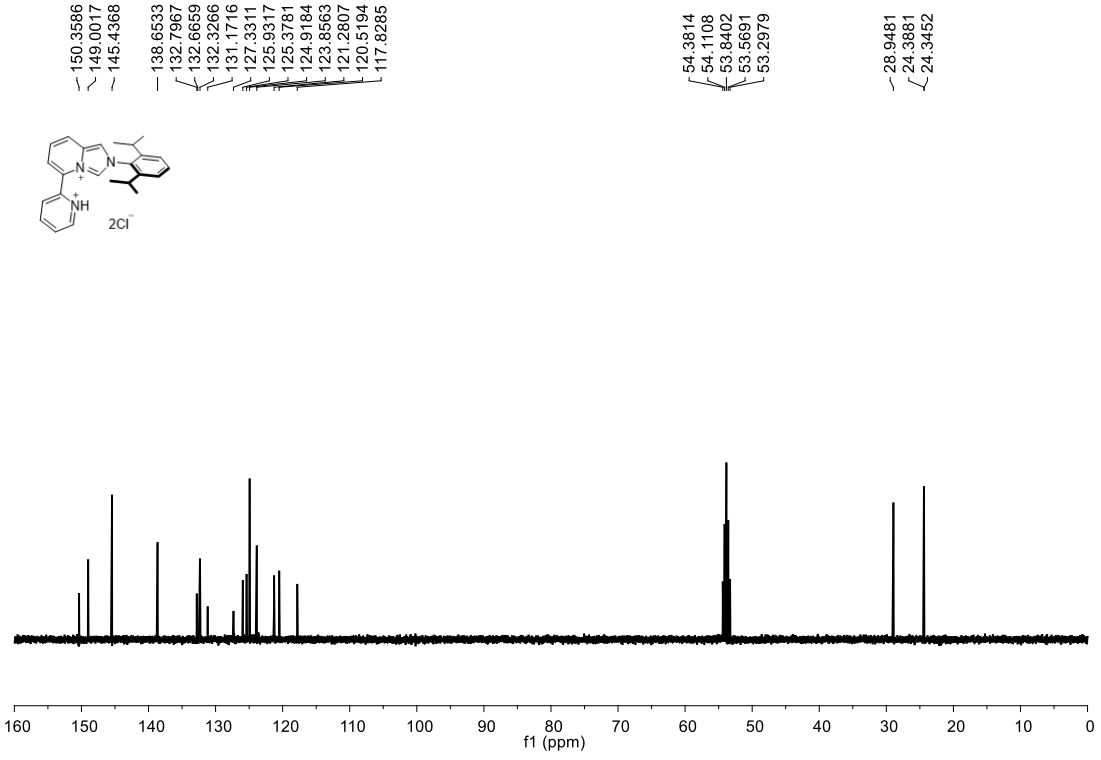

Figure S5 ^{13}C{^{1}H}NMR spectrum of **3** in CD_2Cl_2 at 25 ℃

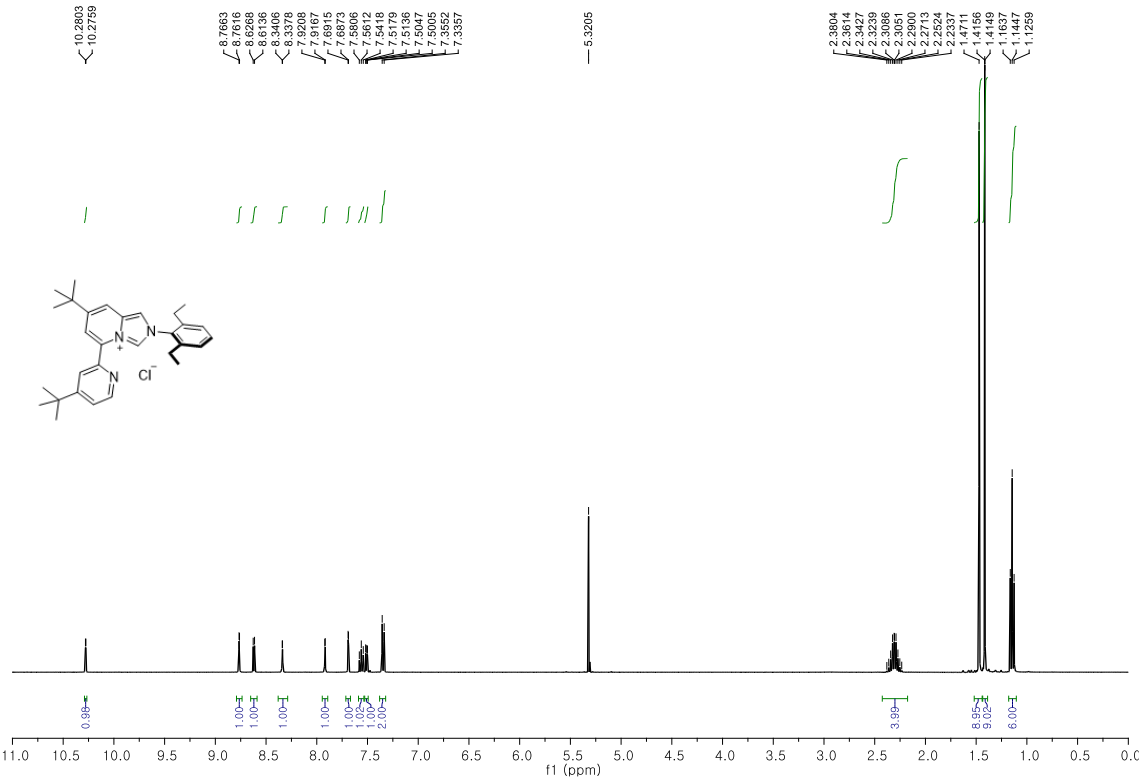

Figure S6 ^{1}H NMR spectrum of **4a** in CD_2Cl_2 at 25 ℃

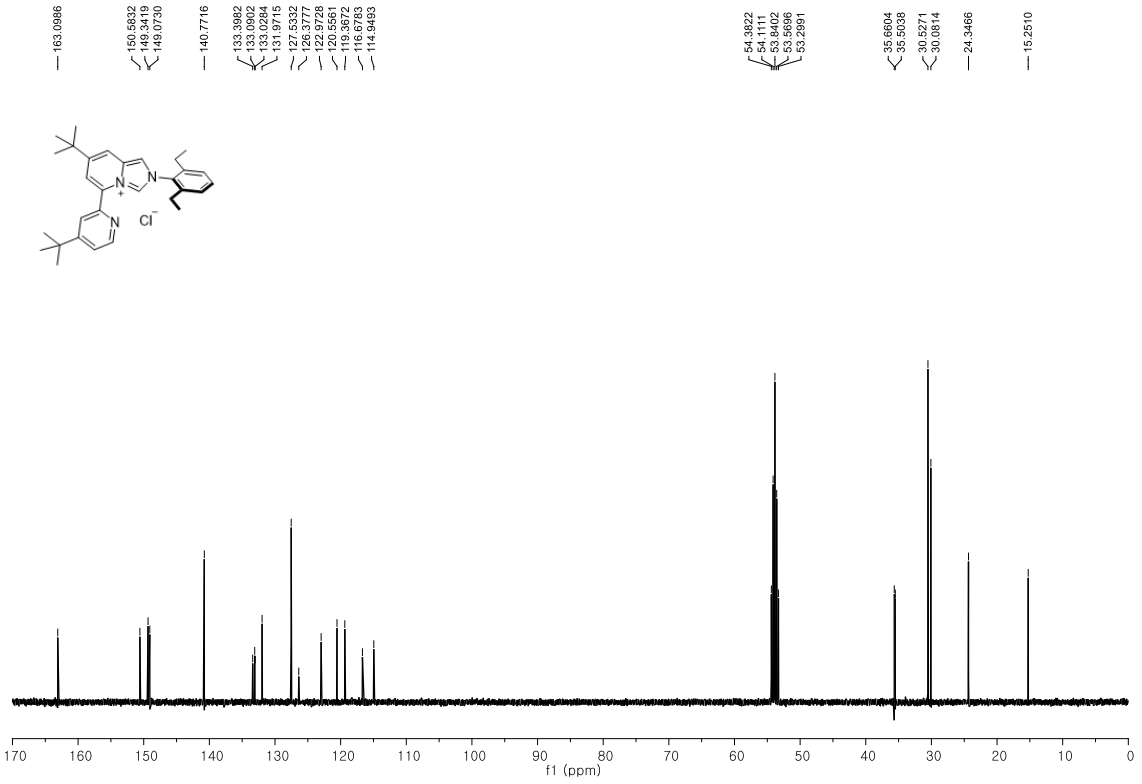

Figure S7 $^{13}C\{^{1}H\}$ NMR spectrum of **4a** in CD_2Cl_2 at 25 ℃

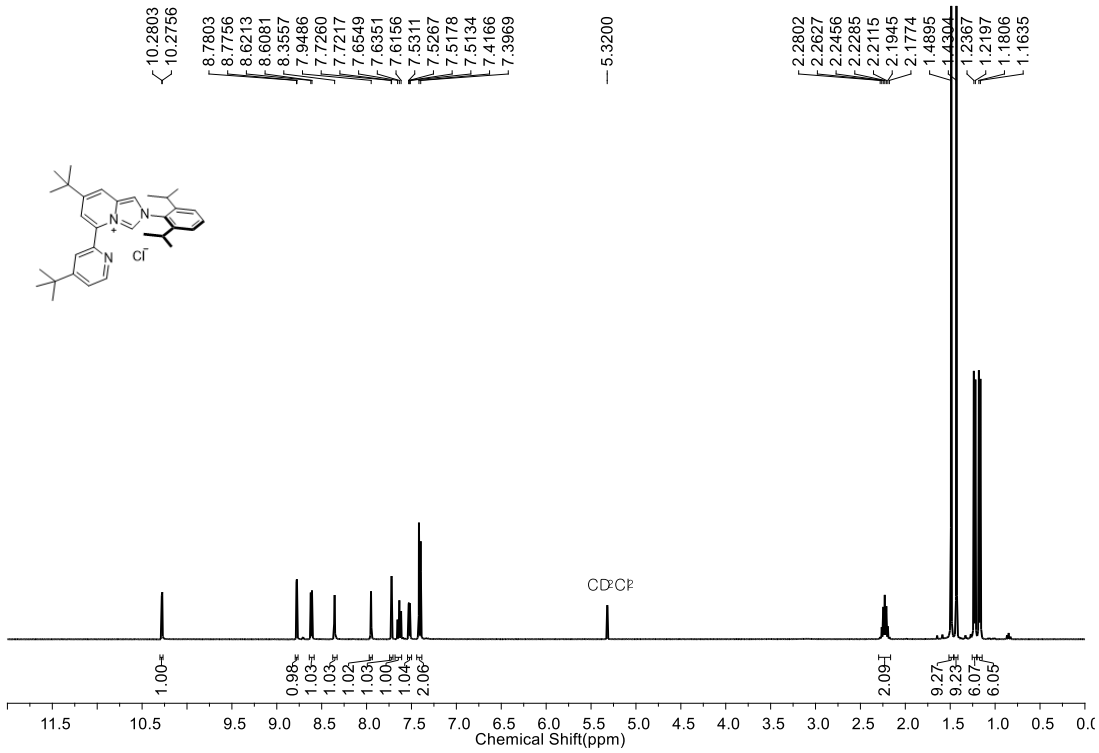

Figure S8 ^{1}H NMR spectrum of **4b** in CD_2Cl_2 at 25 ℃

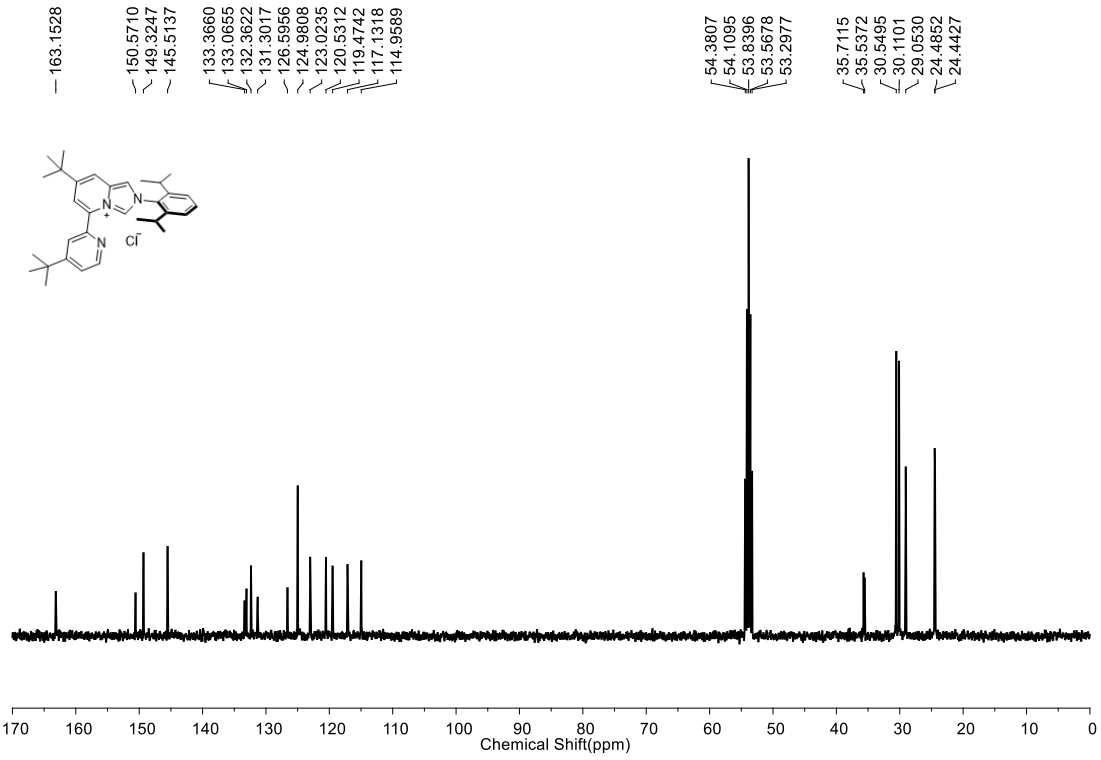

Figure S9 $^{13}C\{^{1}H\}$ NMR spectrum of **4b** in CD_2Cl_2 at 25 ℃

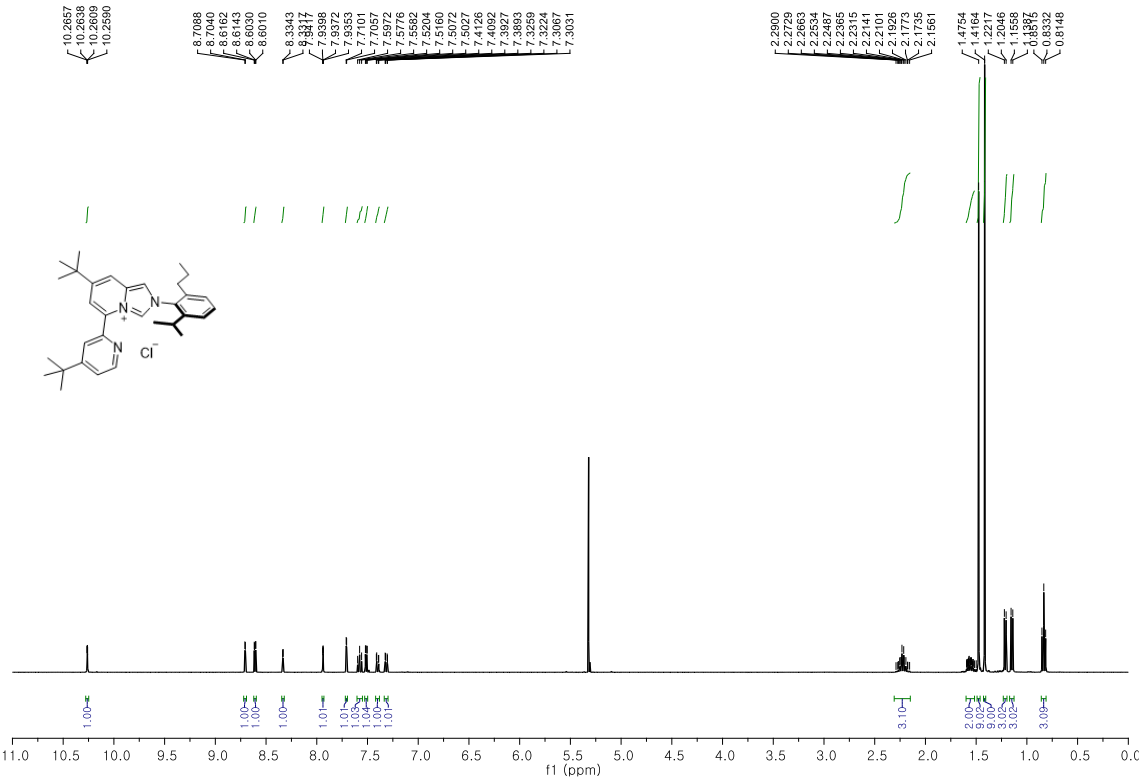

Figure S10 ^{1}H NMR spectrum of **4c** in CD_2Cl_2 at 25 ℃

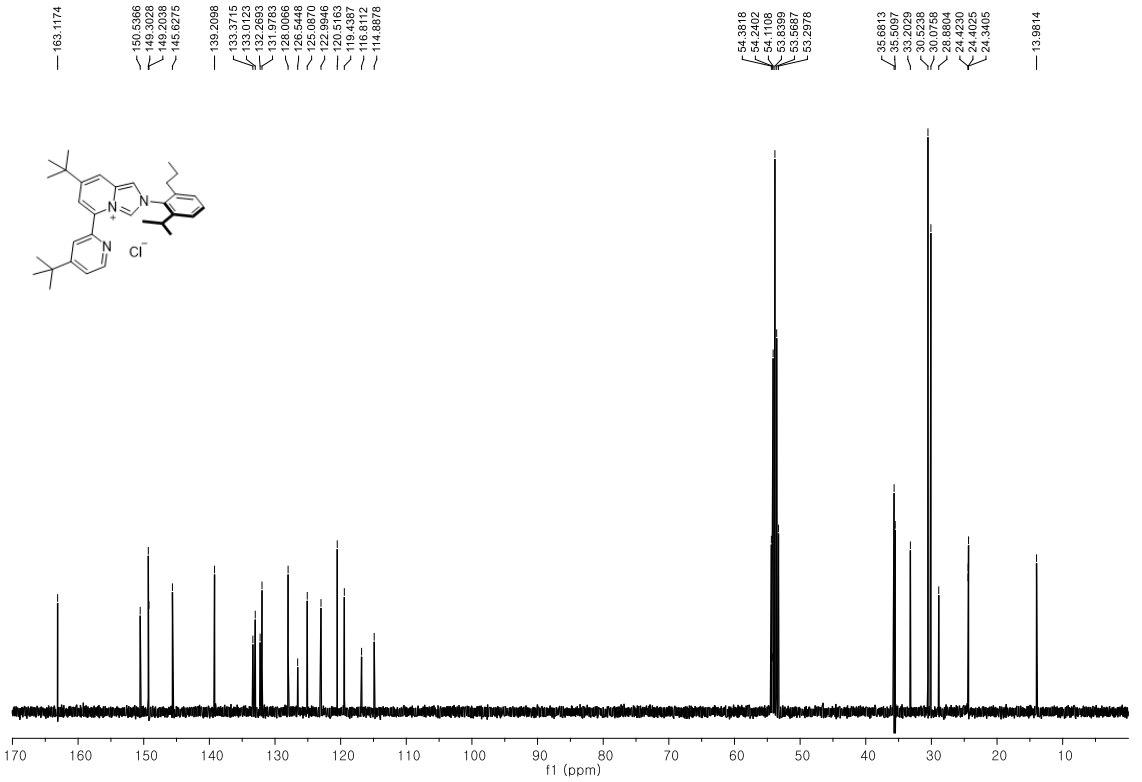

Figure S11 ^{13}C{^{1}H} NMR spectrum of **4c** in CD_2Cl_2 at 25 ℃

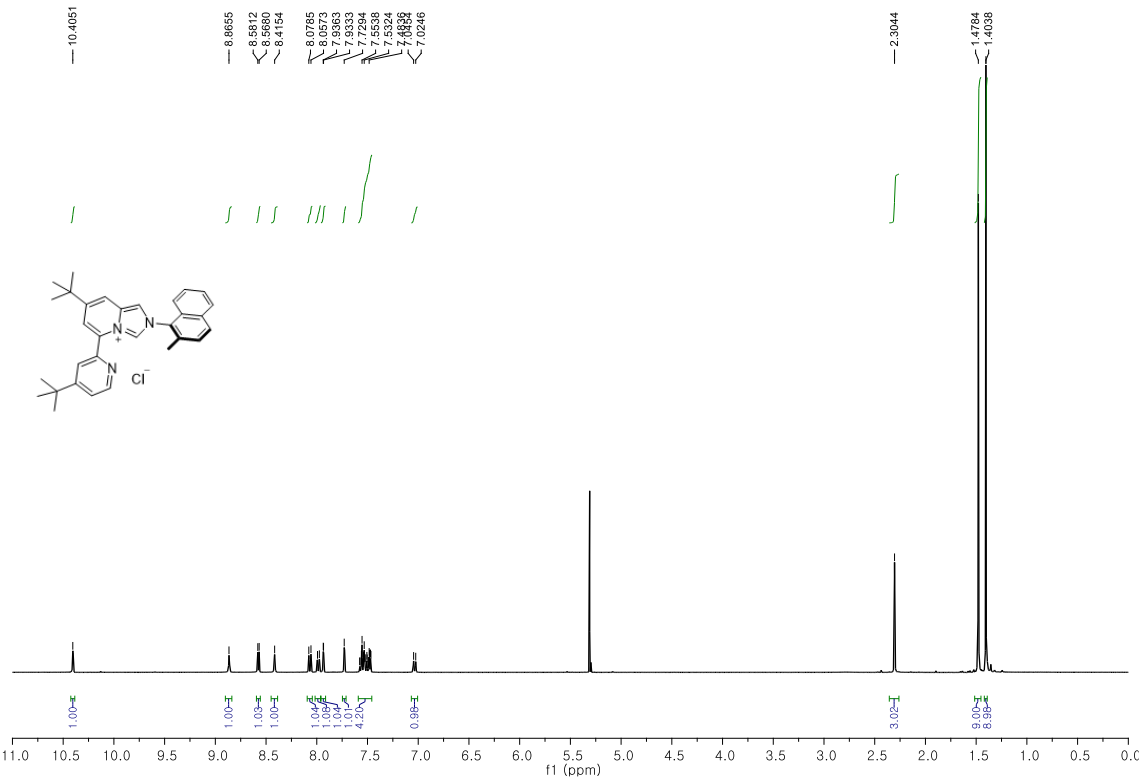

Figure S12 ^{1}H NMR spectrum of **4d** in CD_2Cl_2 at 25 ℃

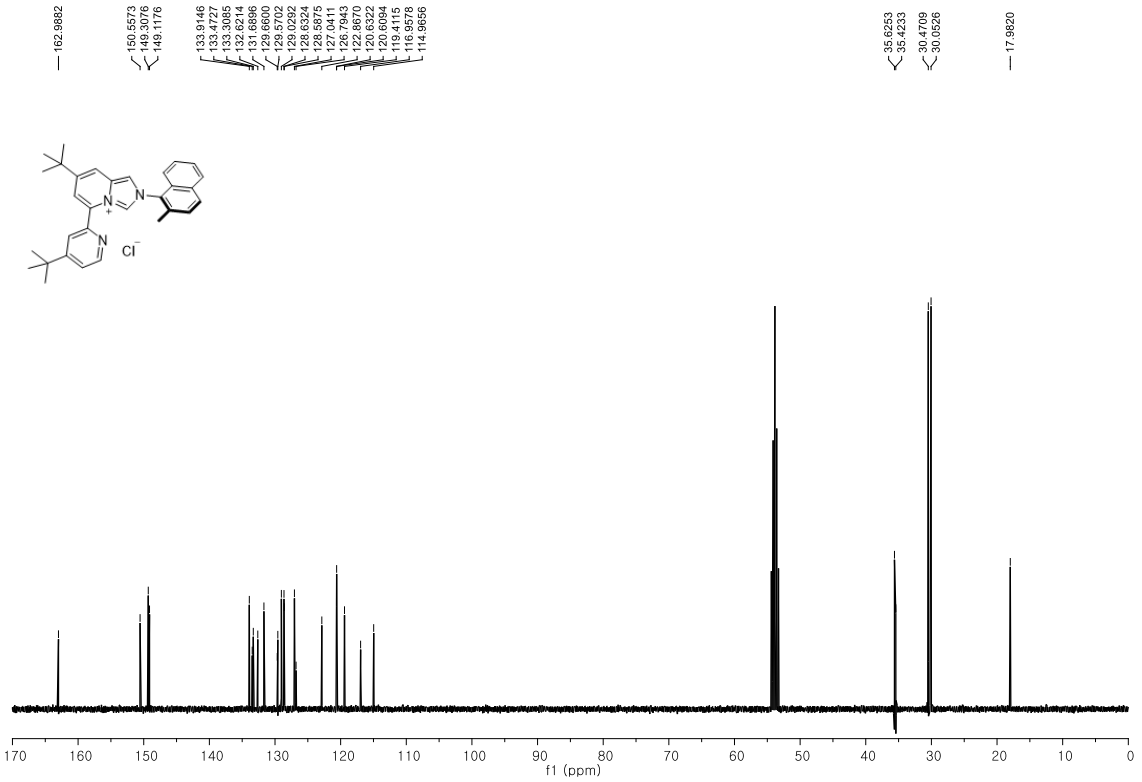

Figure S13 ^{13}C{^{1}H} NMR spectrum of **4d** in CD_2Cl_2 at 25 ℃

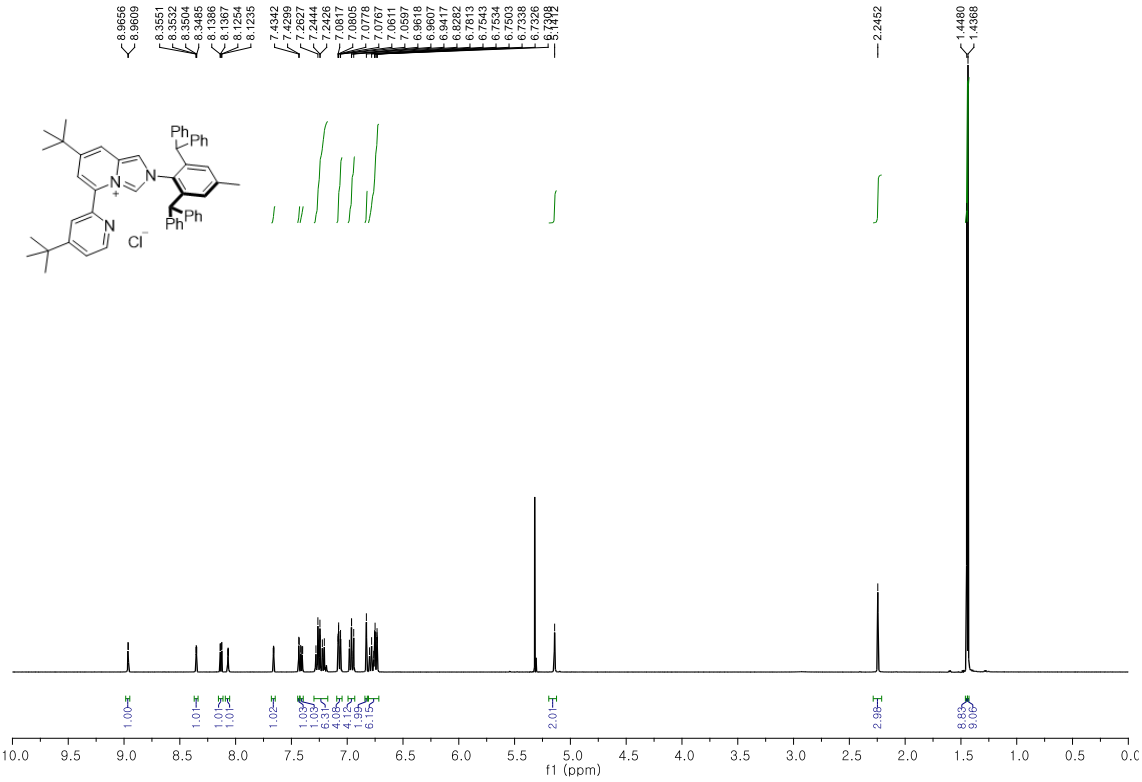

Figure S14 ^{1}H NMR spectrum of **4e** in CD_2Cl_2 at 25 ℃

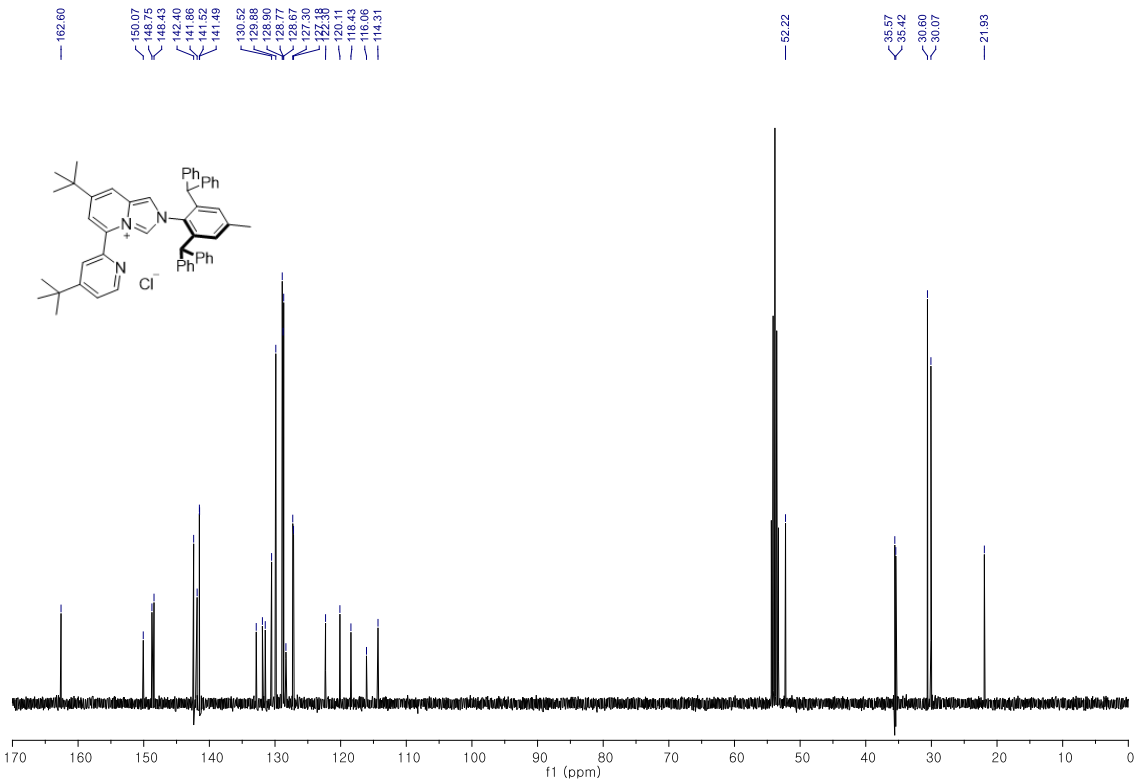

Figure S15 $^{13}C\{^{1}H\}$ NMR spectrum of **4e** in CD_2Cl_2 at 25 ℃

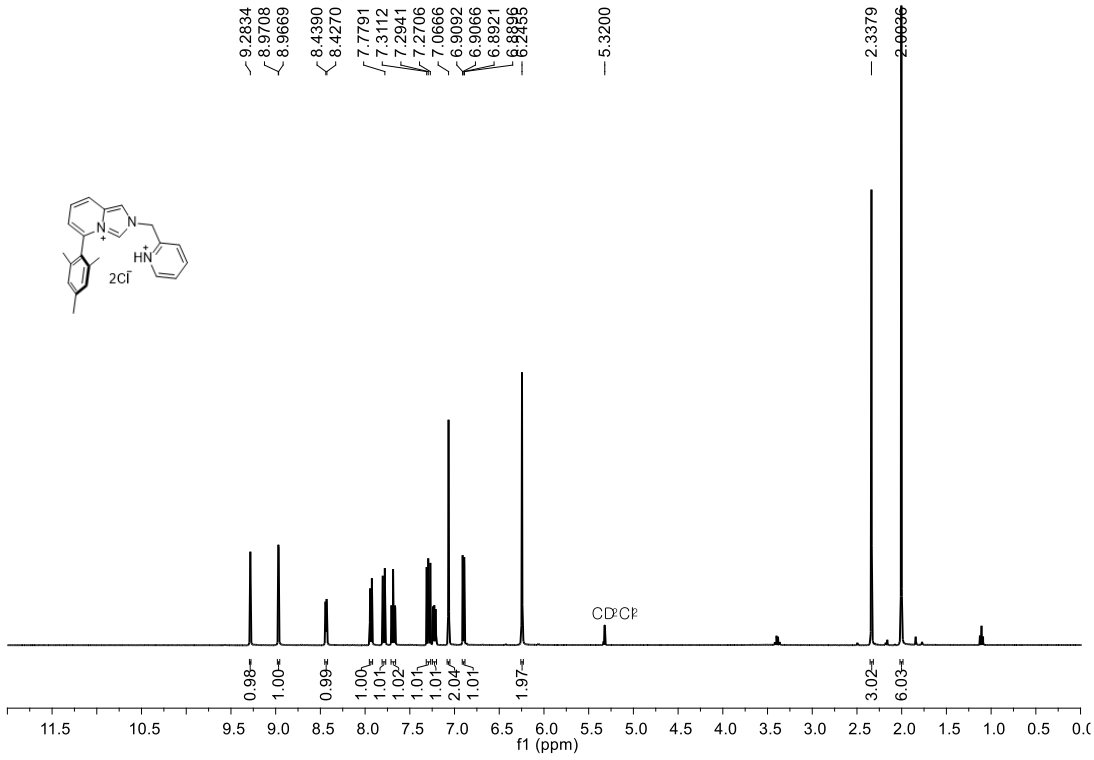

Figure S16 ^{1}H NMR spectrum of **10** in CD_2Cl_2 at 25 ℃

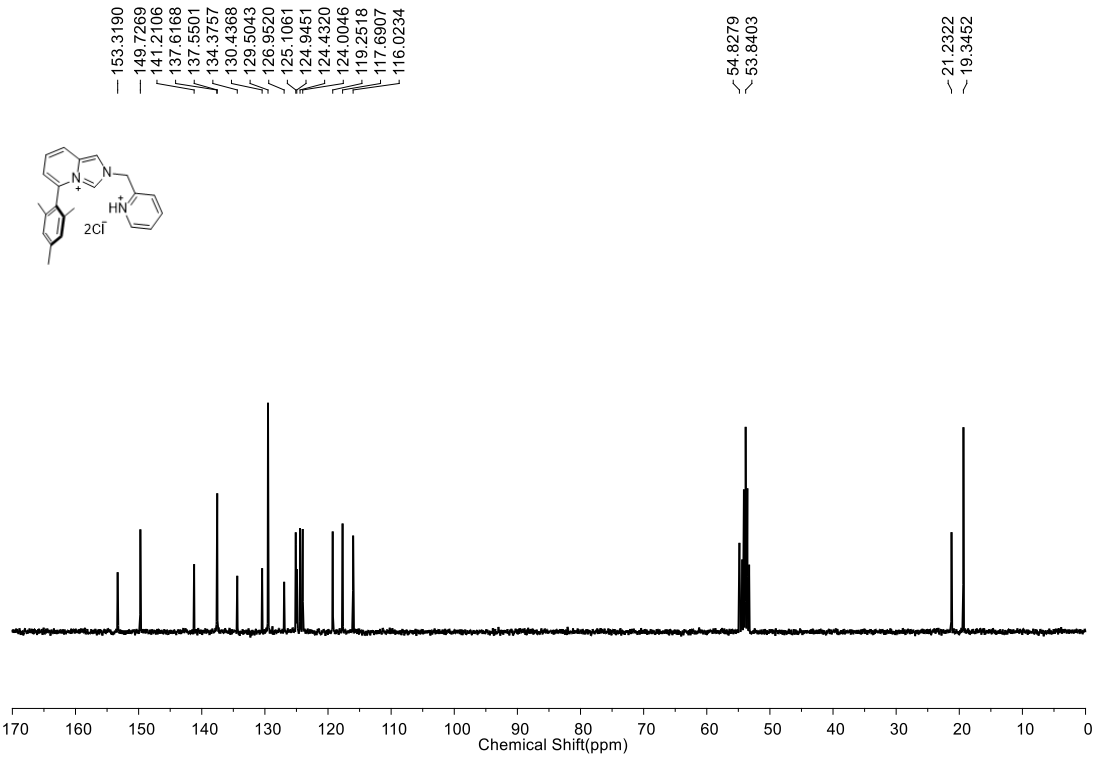

Figure S17 $^{13}C\{^{1}H\}$NMR spectrum of **10** in CD_2Cl_2 at 25 ℃

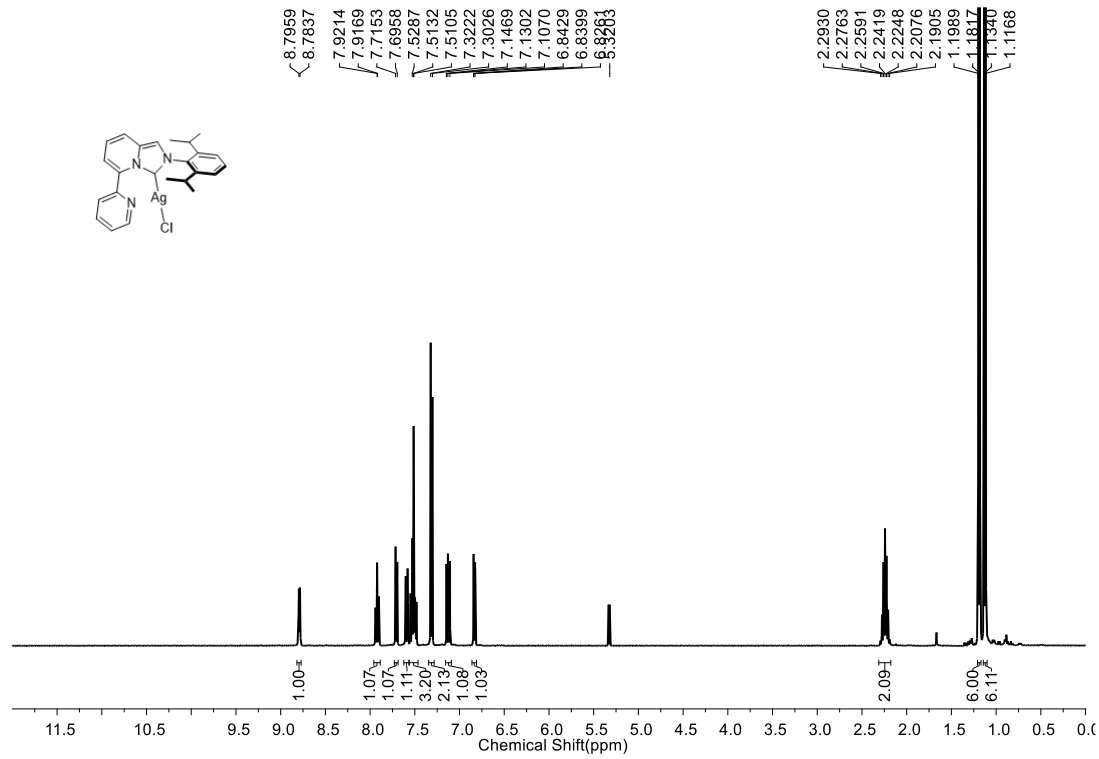

Figure S18 ^{1}H NMR spectrum of **5** in CD_2Cl_2 at 25 ℃

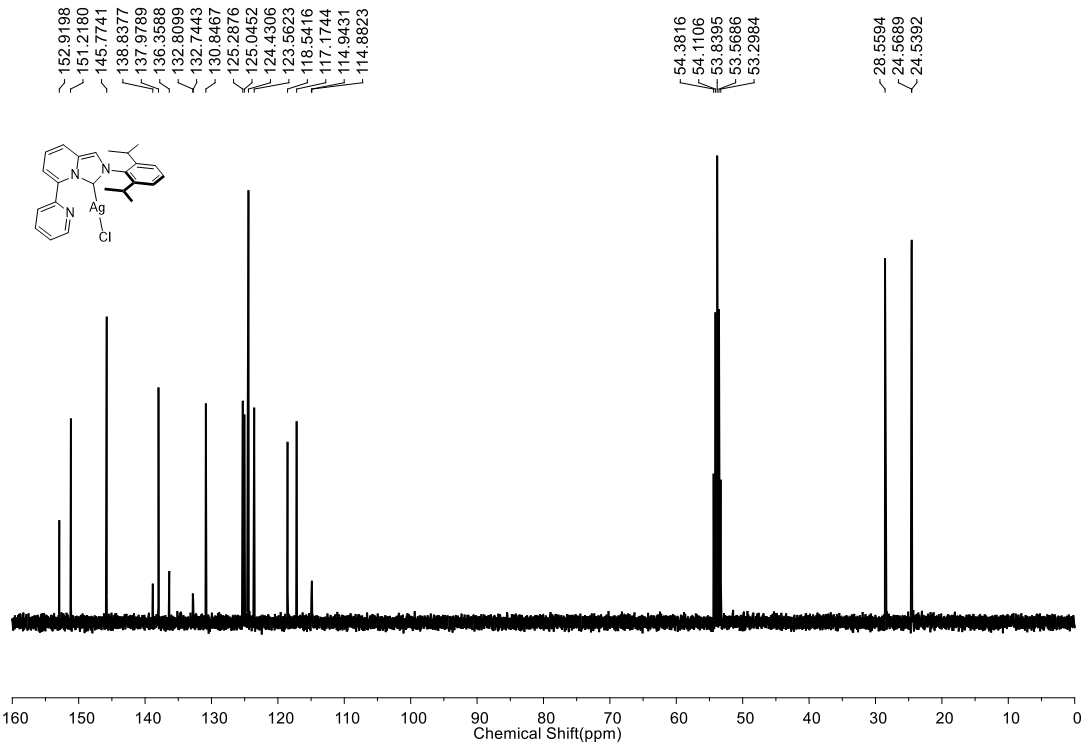

Figure S19 $^{13}C\{^{1}H\}$NMR spectrum of **5** in CD_2Cl_2 at 25 ℃

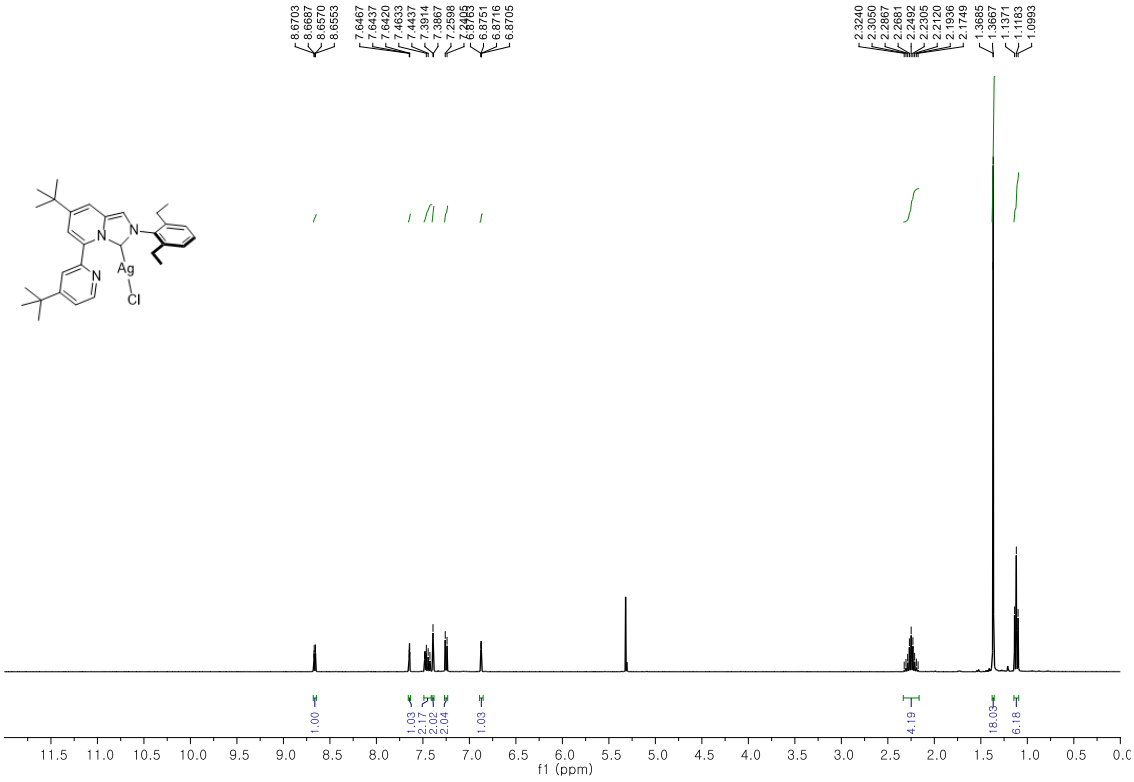

Figure S20 ^{1}H NMR spectrum of **6a** in CD_2Cl_2 at 25 ℃

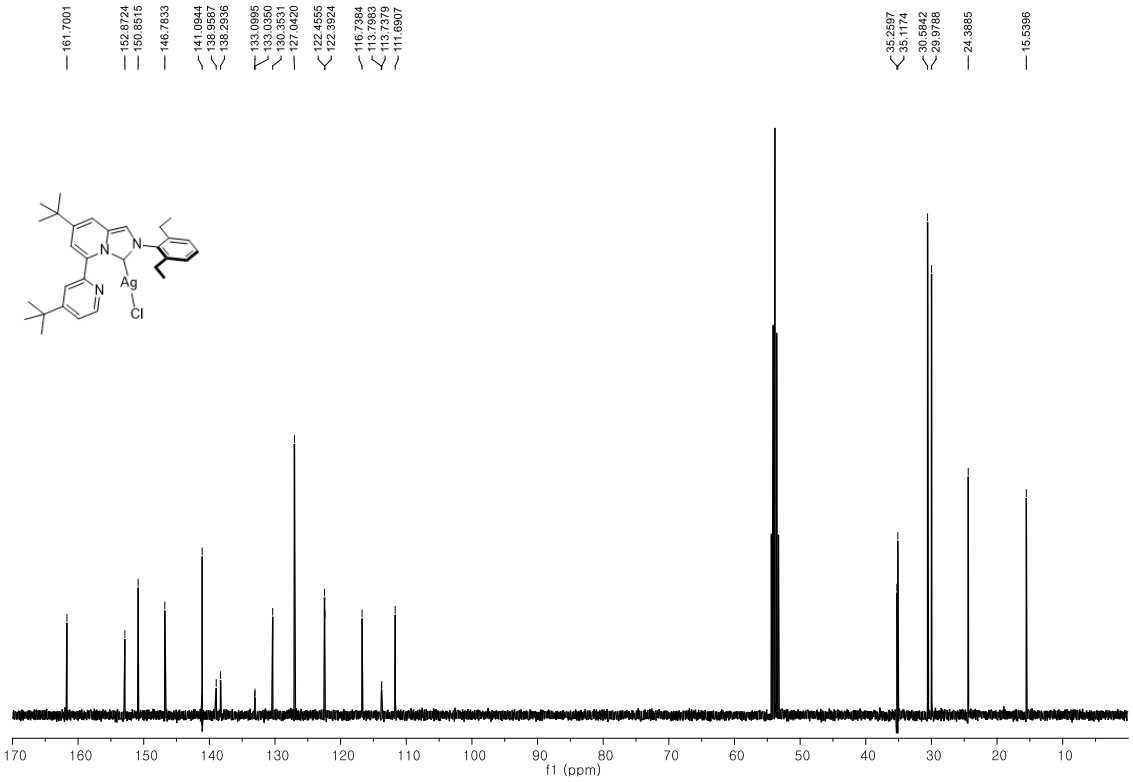

Figure S21 $^{13}C\{^{1}H\}$NMR spectrum of **6a** in CD_2Cl_2 at 25 ℃

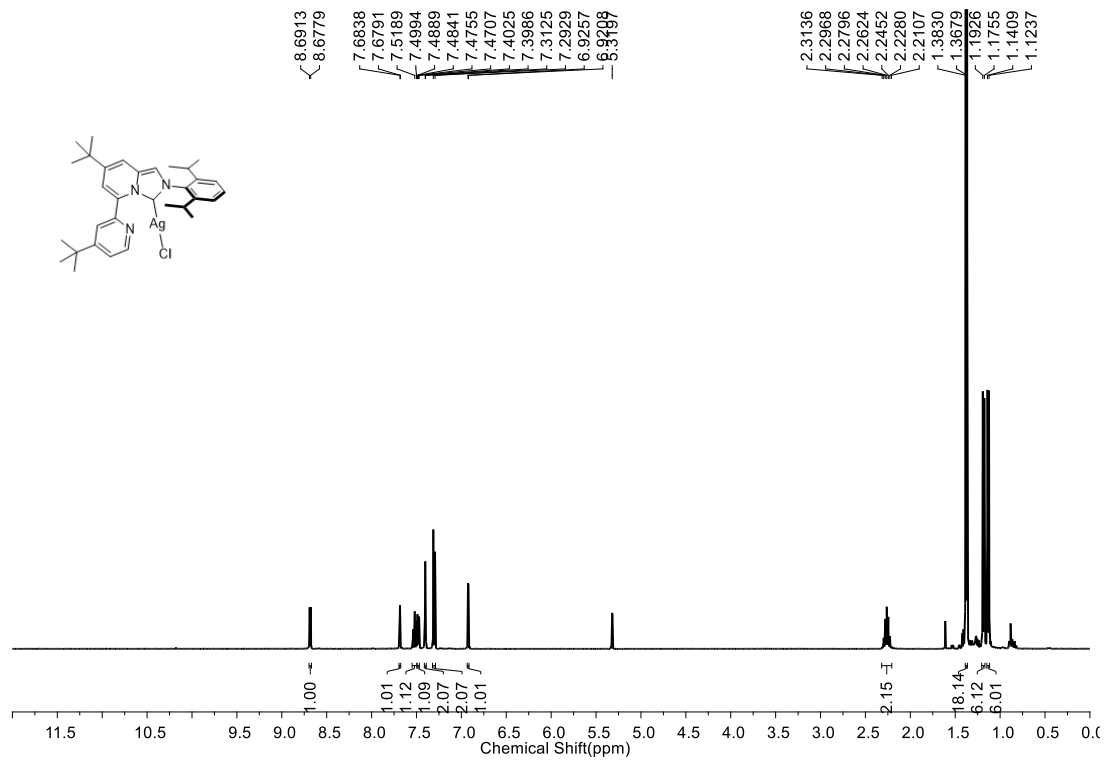

Figure S22 ^{1}H NMR spectrum of **6b** in CD_2Cl_2 at 25 ℃

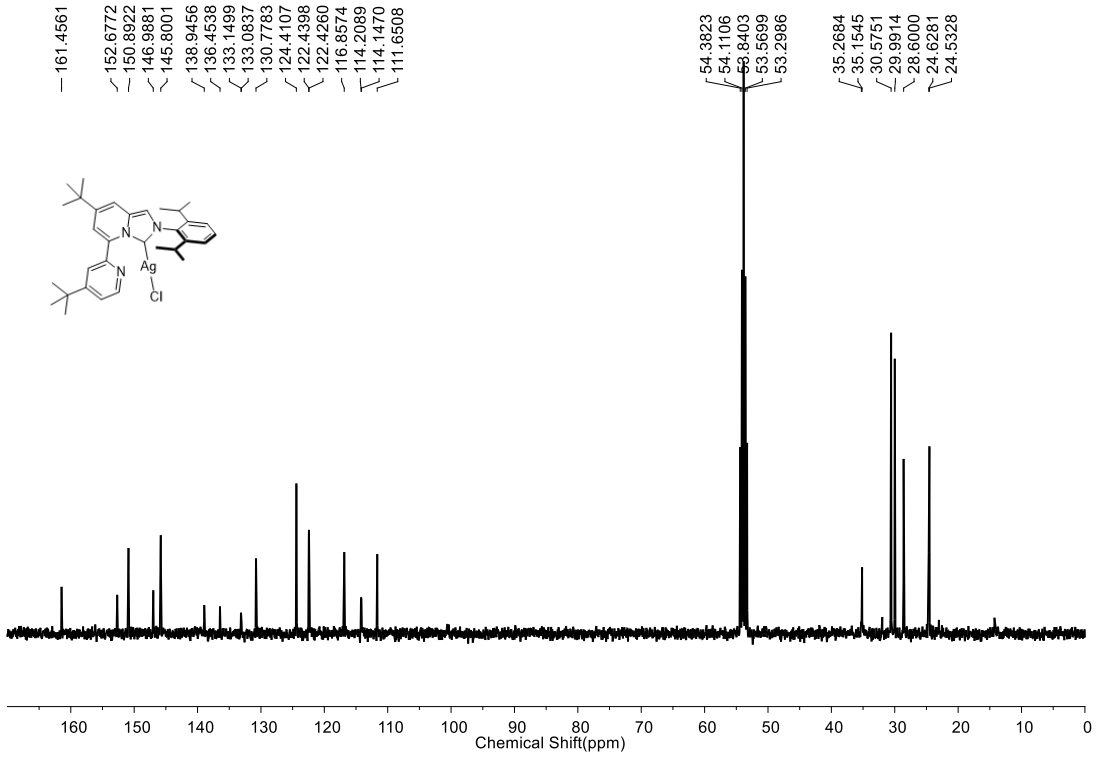

Figure S23 $^{13}C\{^{1}H\}$NMR spectrum of **6b** in CD_2Cl_2 at 25 ℃

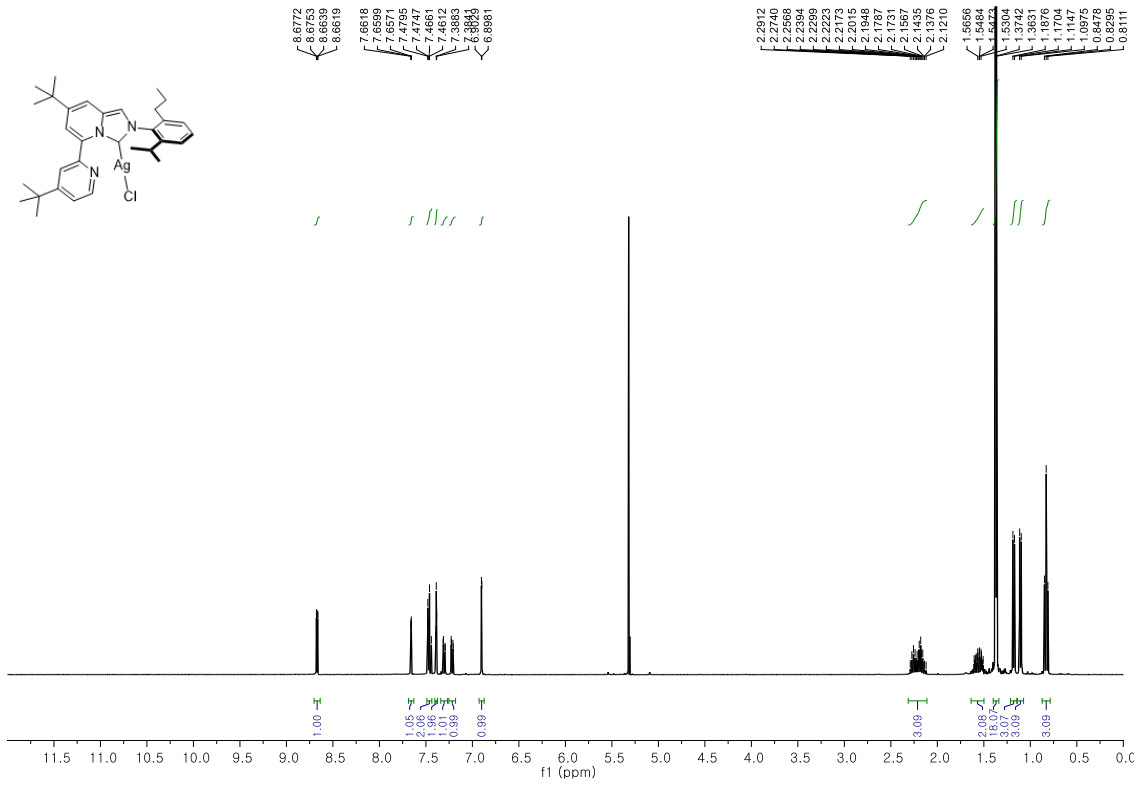

Figure S24 ^{1}H NMR spectrum of **6c** in CD_2Cl_2 at 25 ℃

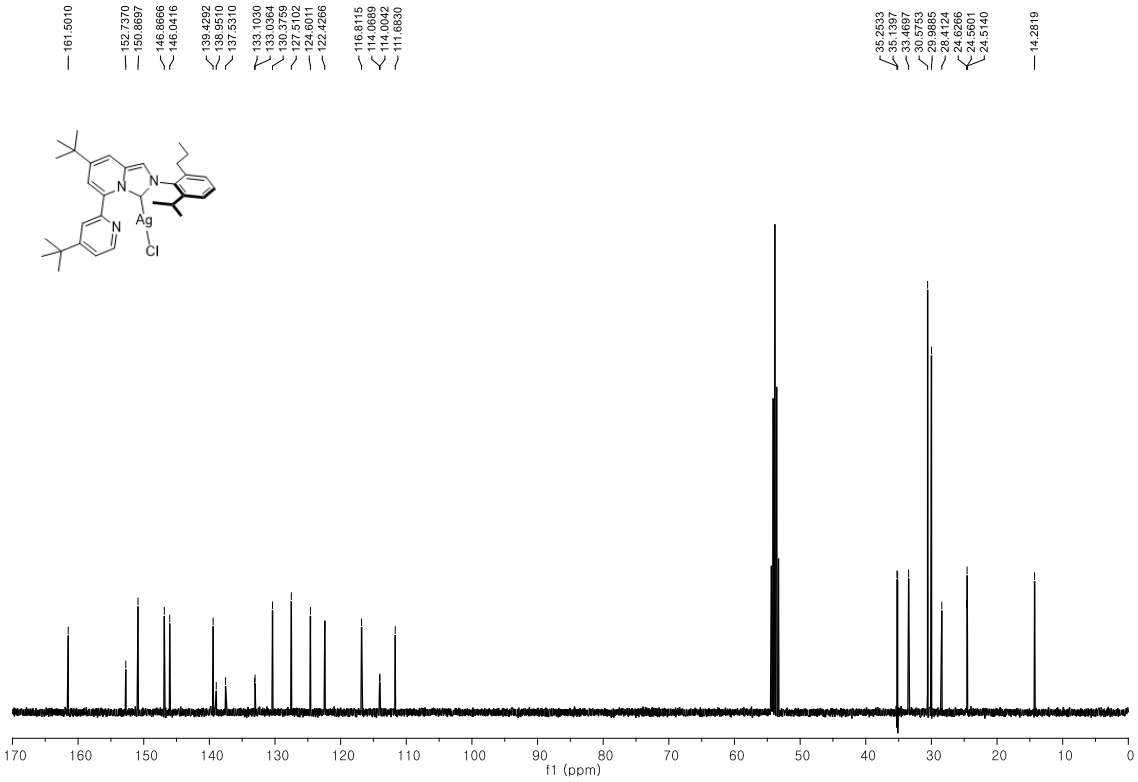

Figure S25 $^{13}C\{^{1}H\}$NMR spectrum of **6c** in CD_2Cl_2 at 25 ℃

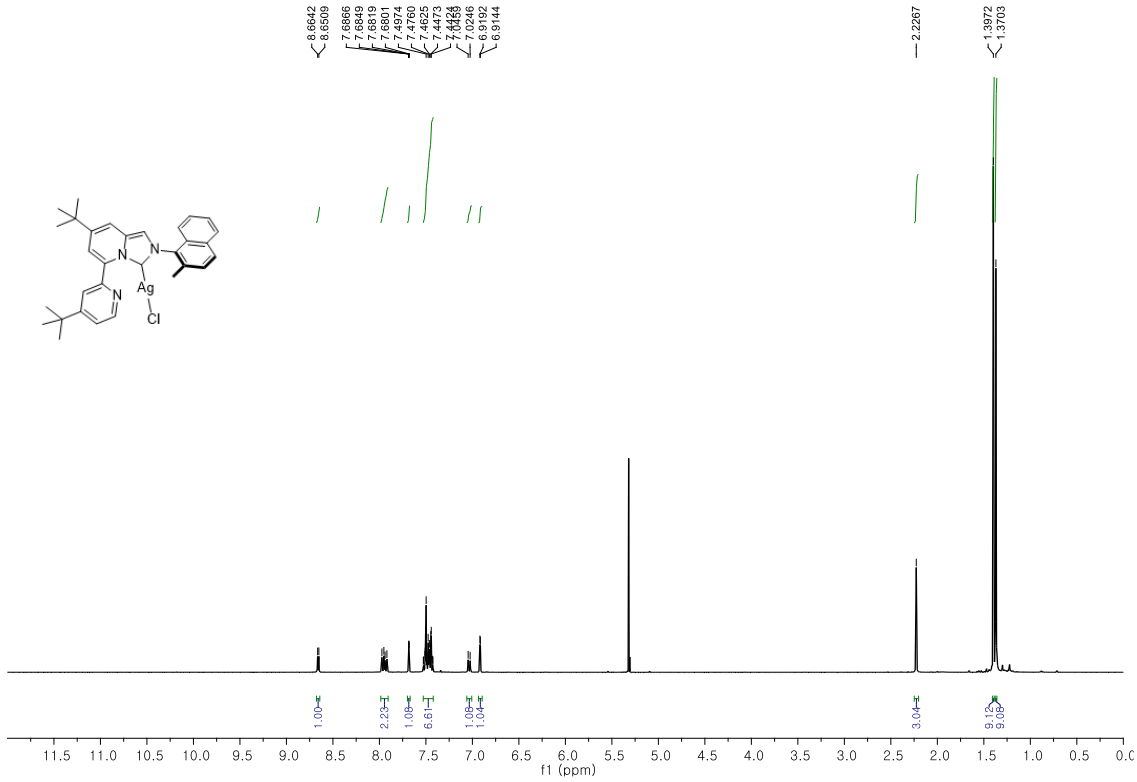

Figure S26 ^{1}H NMR spectrum of **6d** in CD_2Cl_2 at 25 ℃

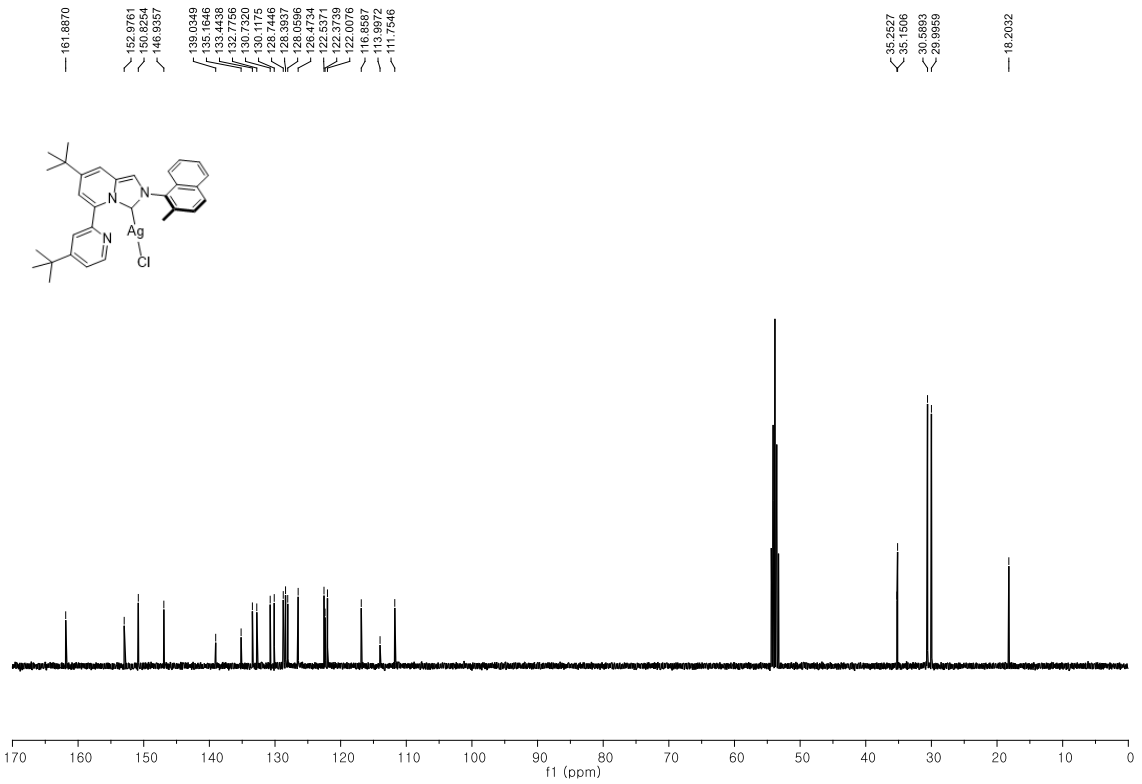

Figure S27 $^{13}C\{^{1}H\}$NMR spectrum of **6d** in CD_2Cl_2 at 25 ℃

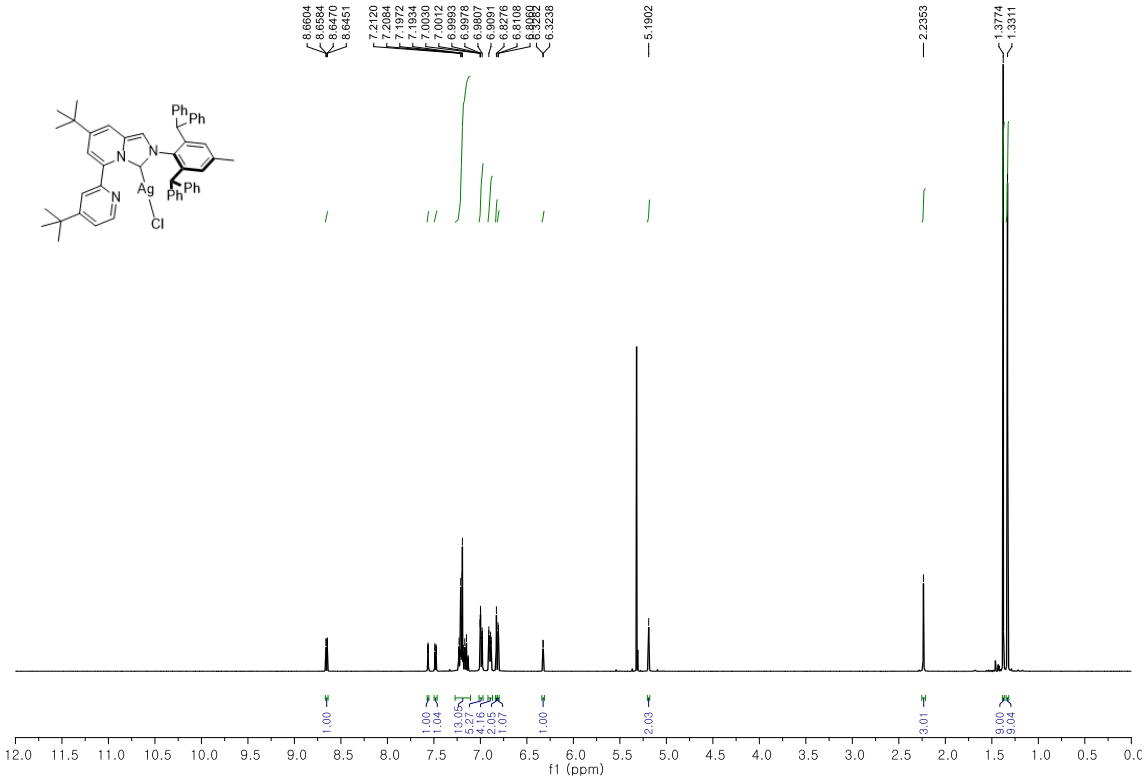

Figure S28 ^{1}H NMR spectrum of **6e** in CD_2Cl_2 at 25 ℃

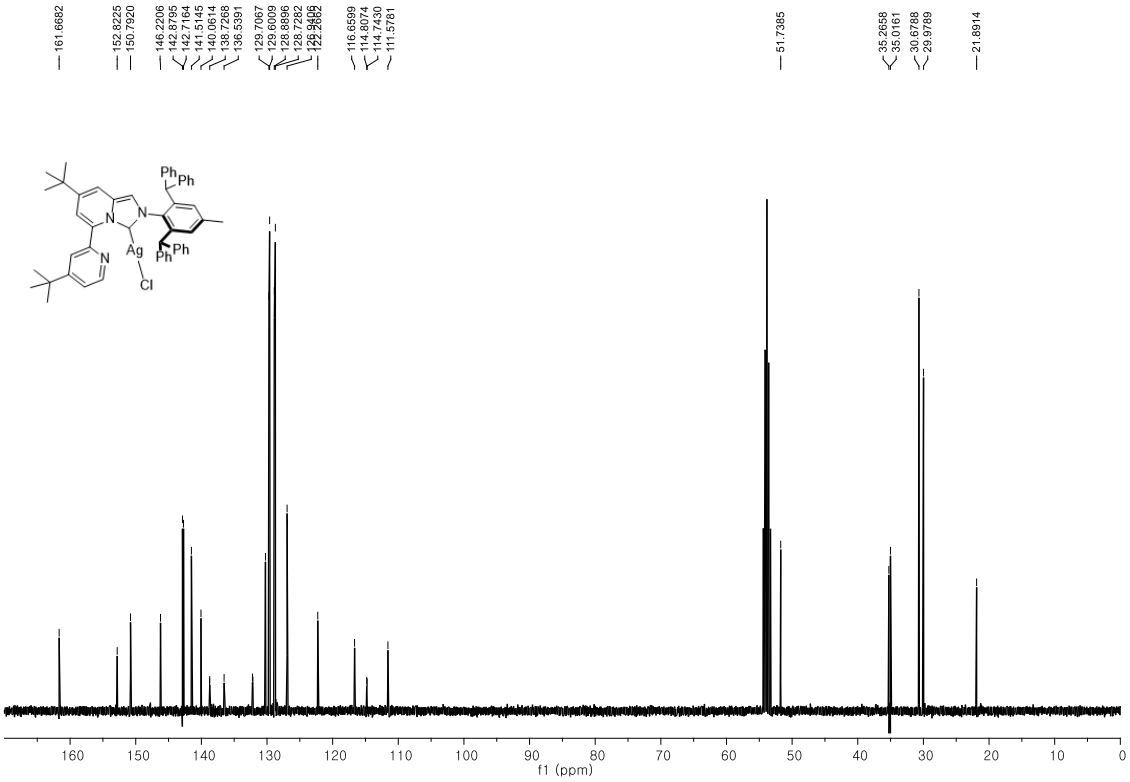

Figure S29 $^{13}C\{^{1}H\}$NMR spectrum of **6e** in CD_2Cl_2 at 25 ℃

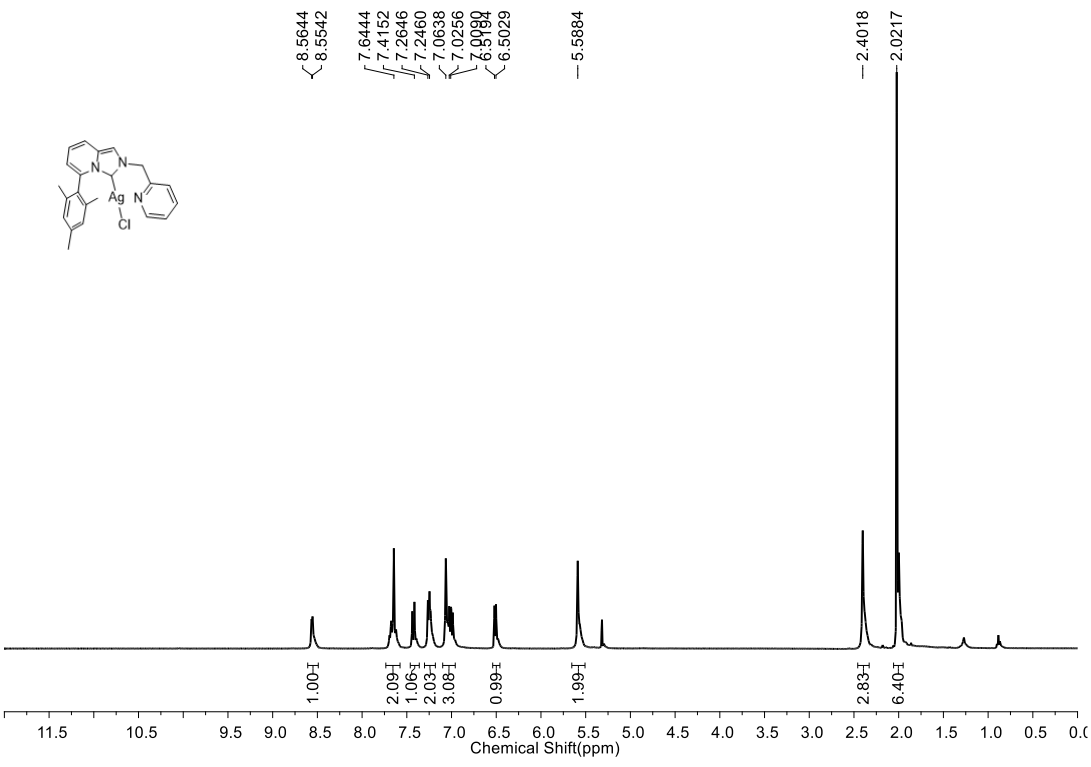

Figure S30 ^{1}H NMR spectrum of **11** in CD_2Cl_2 at 25 ℃

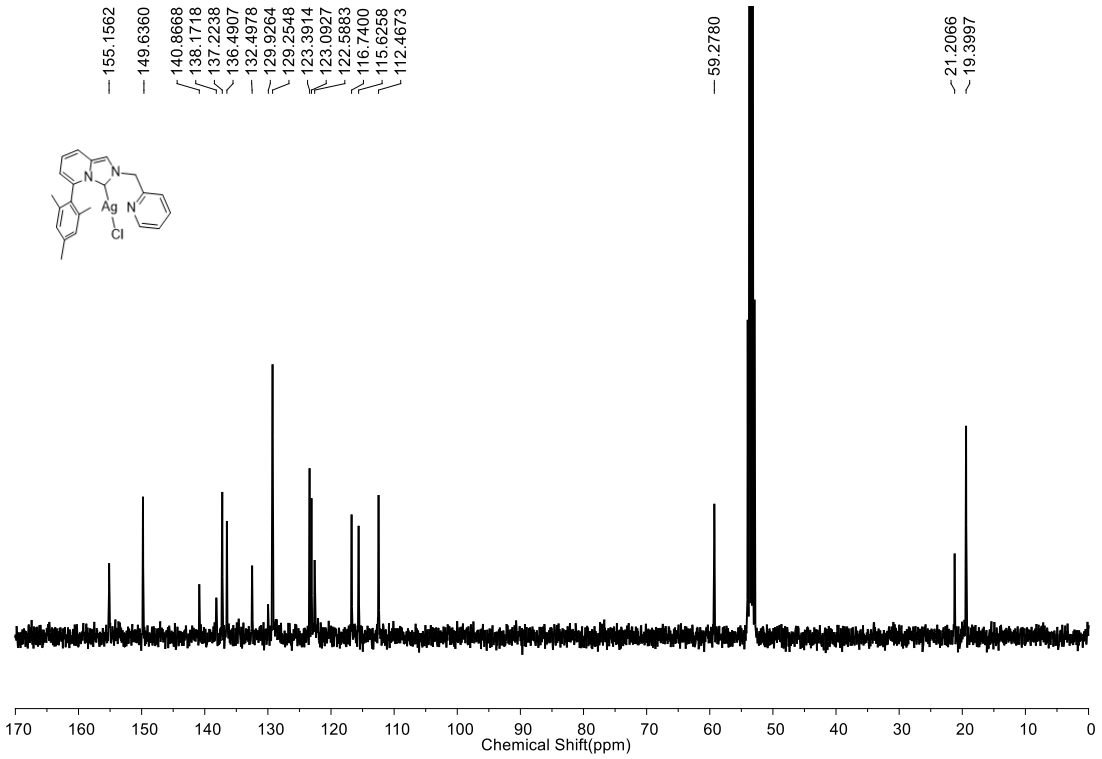

Figure S31 $^{13}C\{^{1}H\}$NMR spectrum of **11** in CD_2Cl_2 at 25 ℃

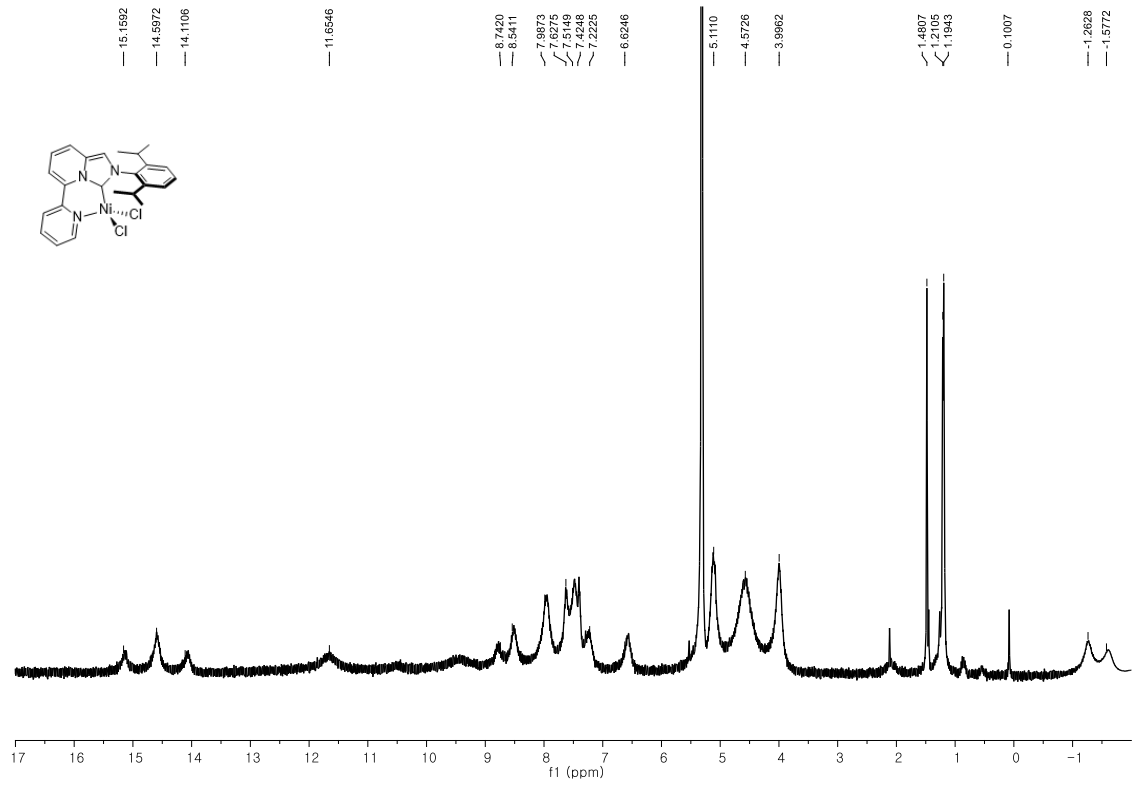

Figure S32 ^{1}H NMR spectrum of **7** in CD_2Cl_2 at 25 ℃

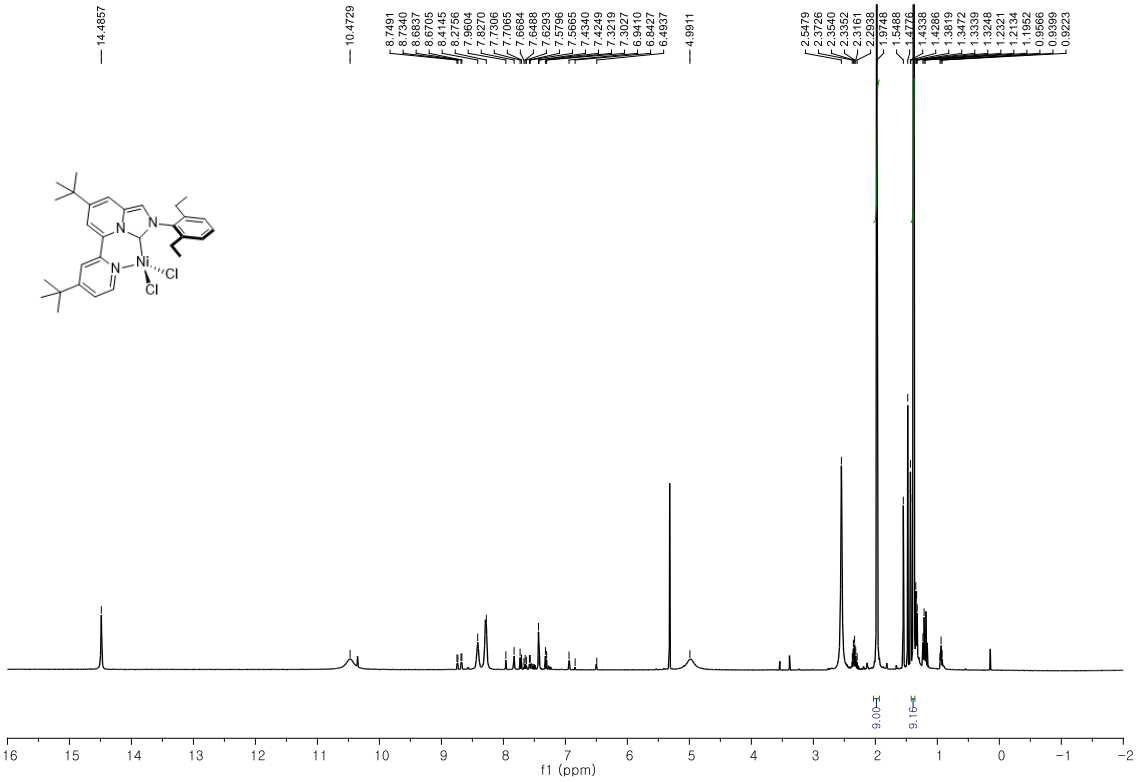

Figure S33 ^{1}H NMR spectrum of **8a** in CD_2Cl_2 at 25 ℃

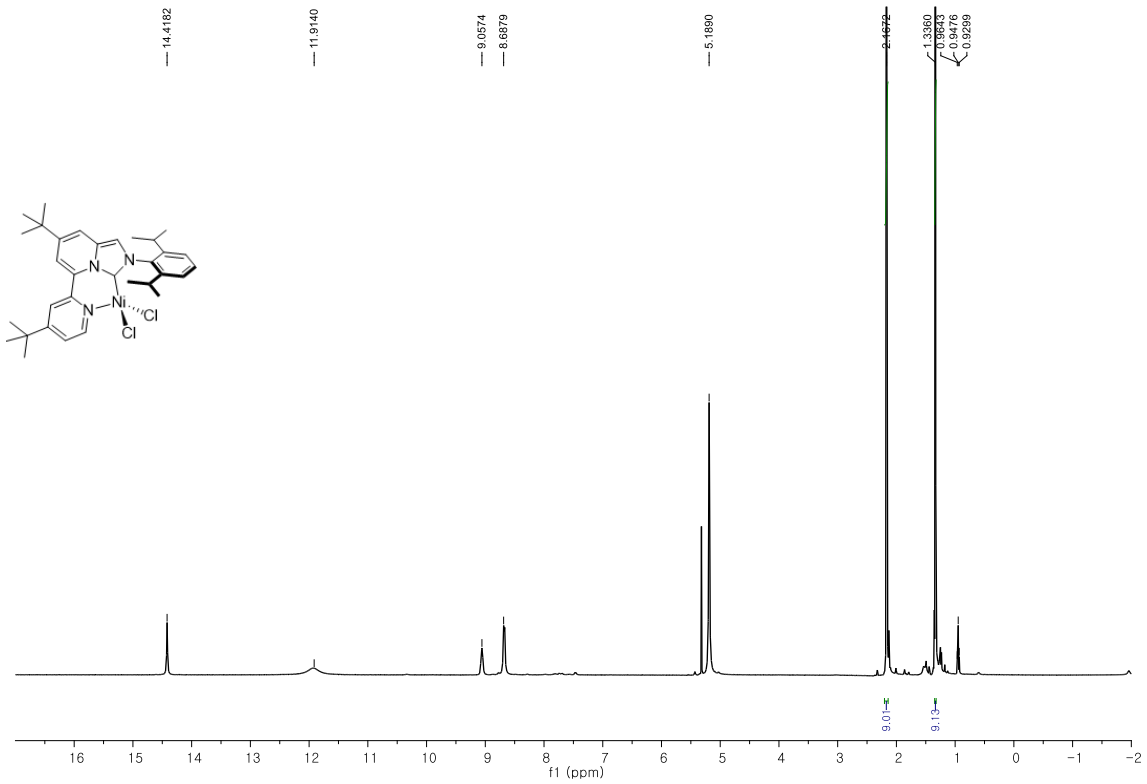

Figure S34 ^{1}H NMR spectrum of **8b** in CD_2Cl_2 at 25 ℃

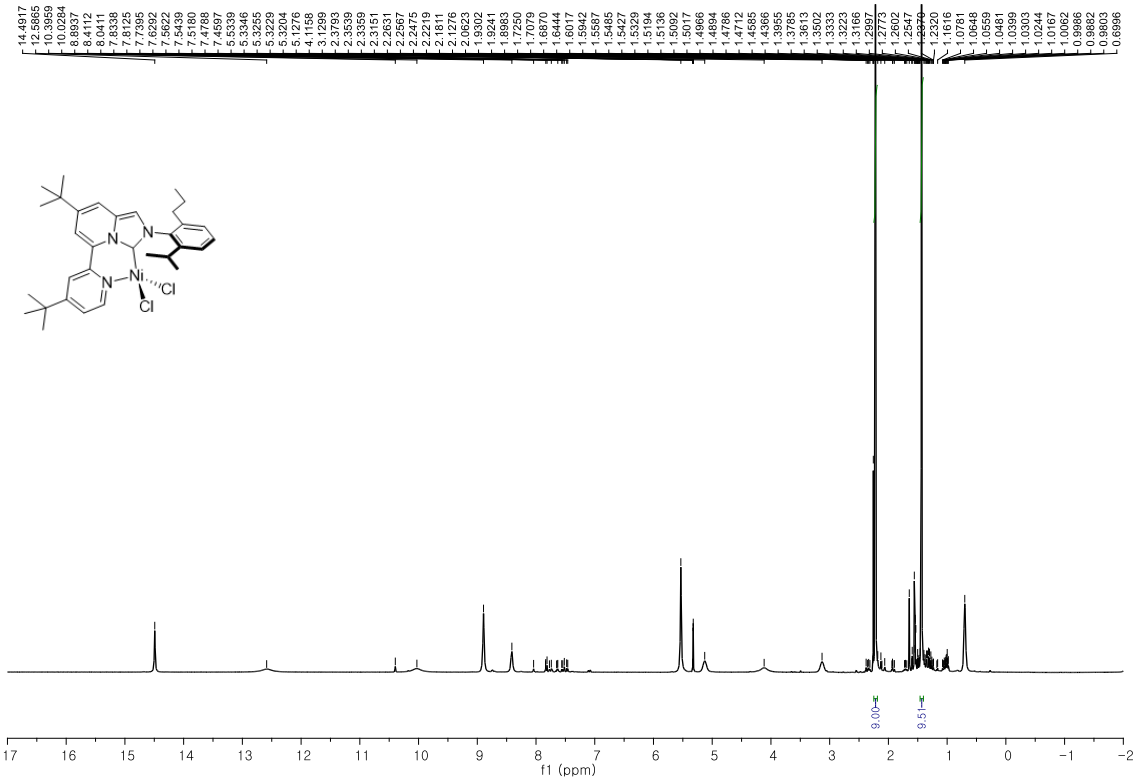

Figure S35 ^{1}H NMR spectrum of **8c** in CD_2Cl_2 at 25 ℃

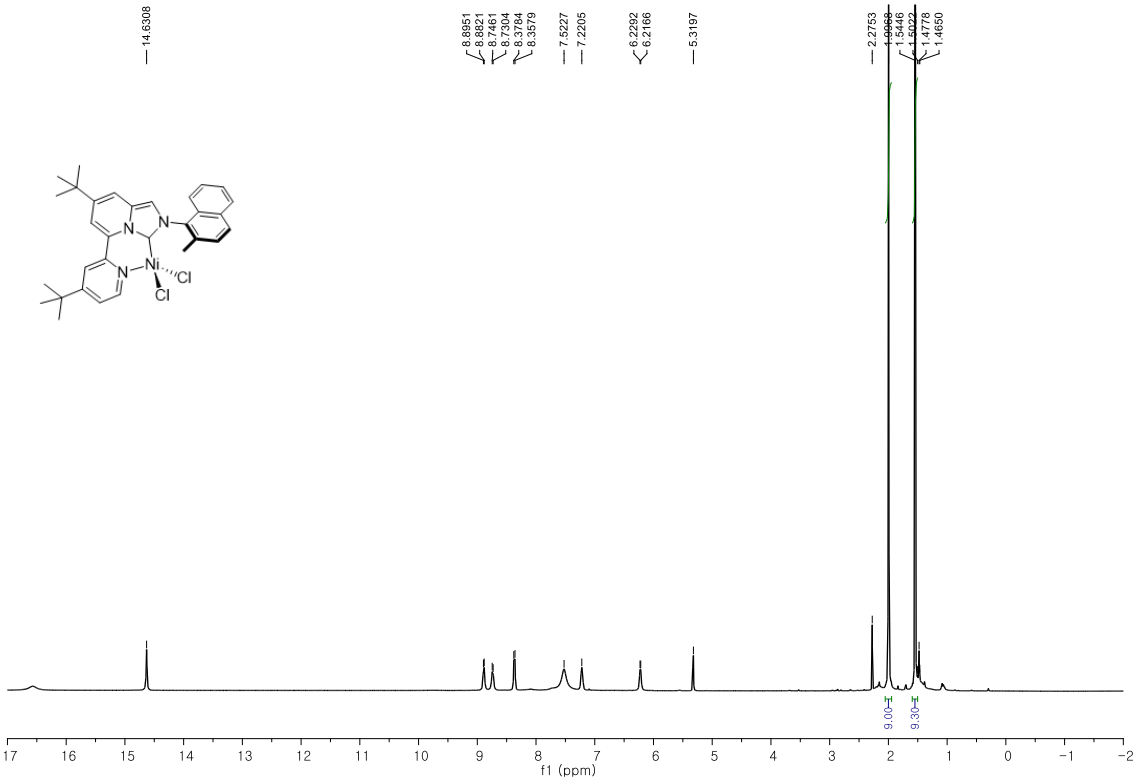

Figure S36 ^{1}H NMR spectrum of **8d** in CD_2Cl_2 at 25 ℃

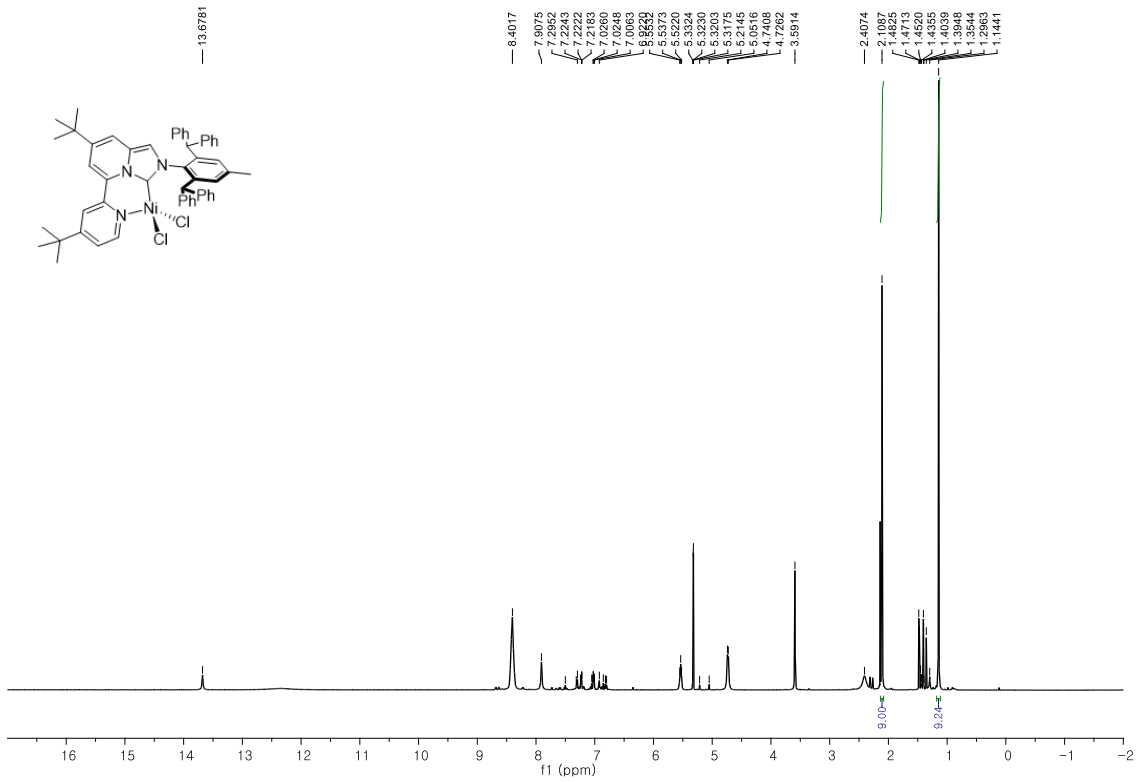

Figure S37 ^{1}H NMR spectrum of **8e** in CD_2Cl_2 at 25 ℃

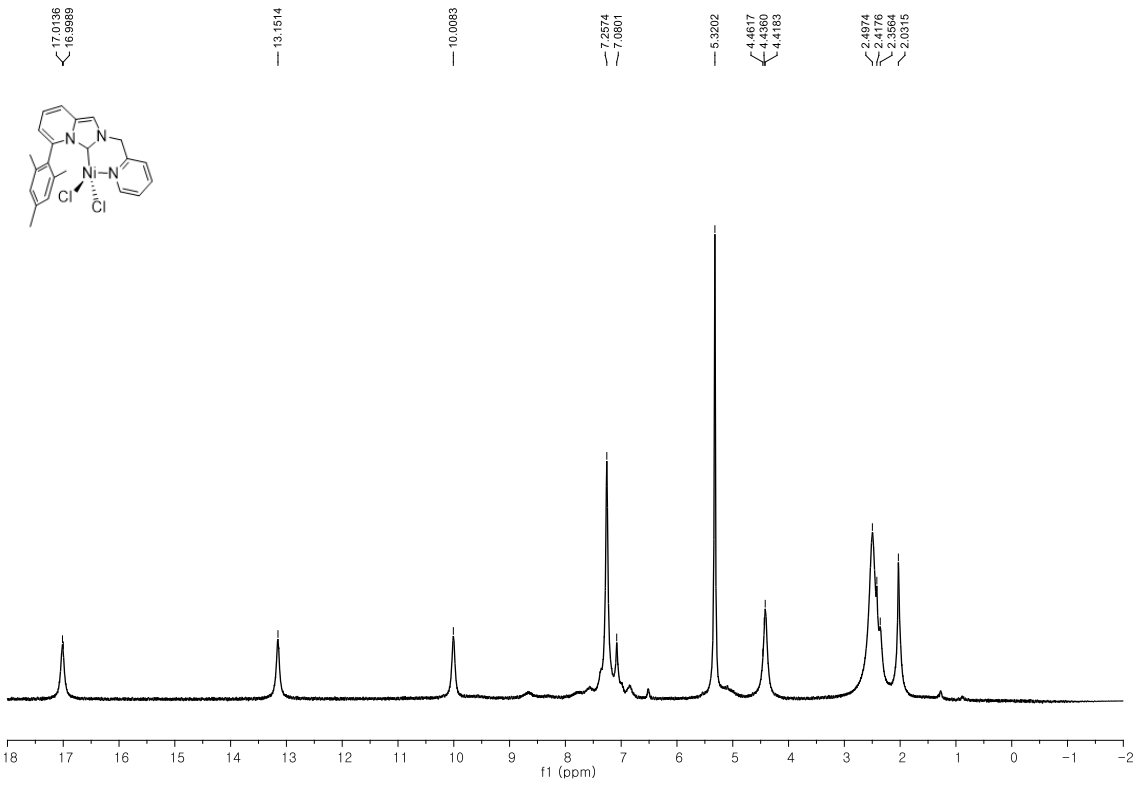

Figure S39 ^{1}H NMR spectrum of **12** in CD_2Cl_2 at 25 ℃

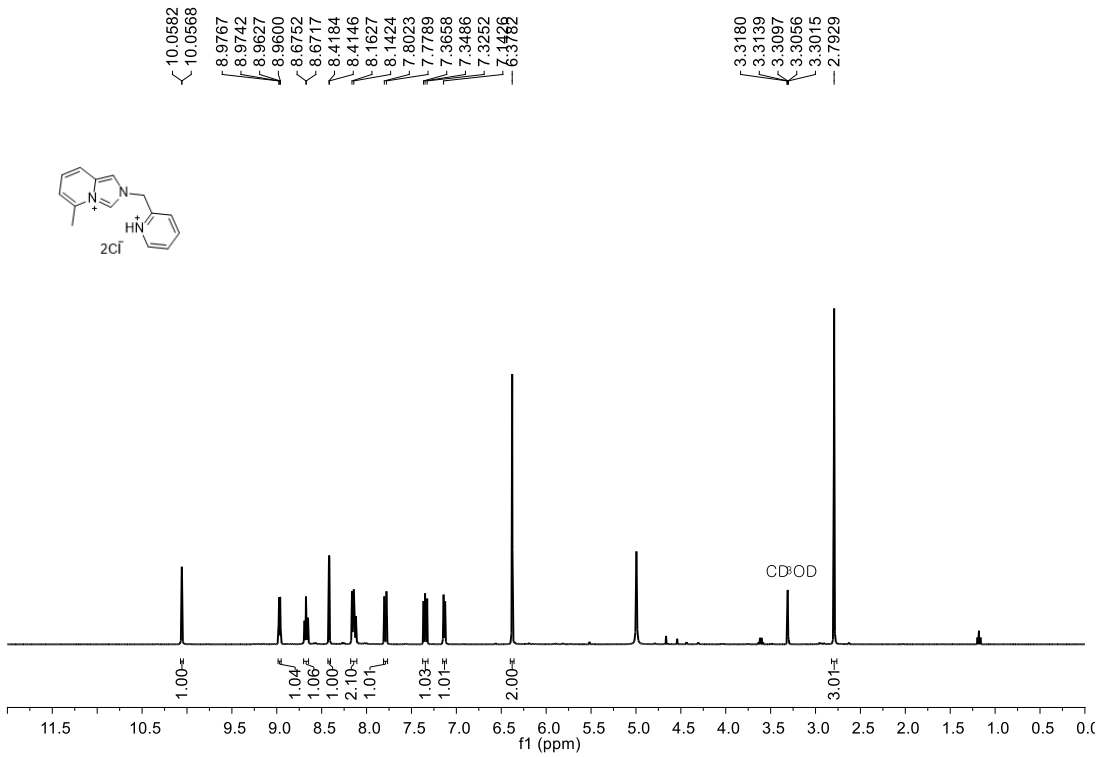

Figure S40 ^{1}H NMR spectrum of **B** in CD_3OD at 25 ℃

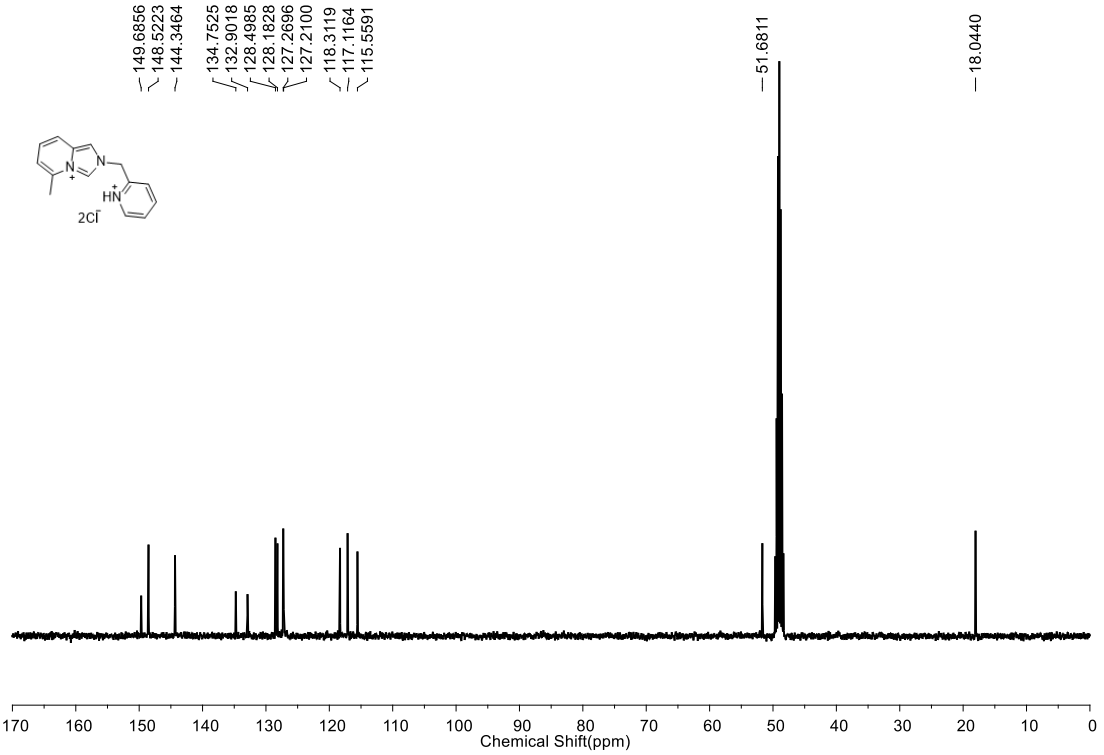

Figure S41 $^{13}C\{^{1}H\}$NMR spectrum of **B** in CD_3OD at 25 ℃

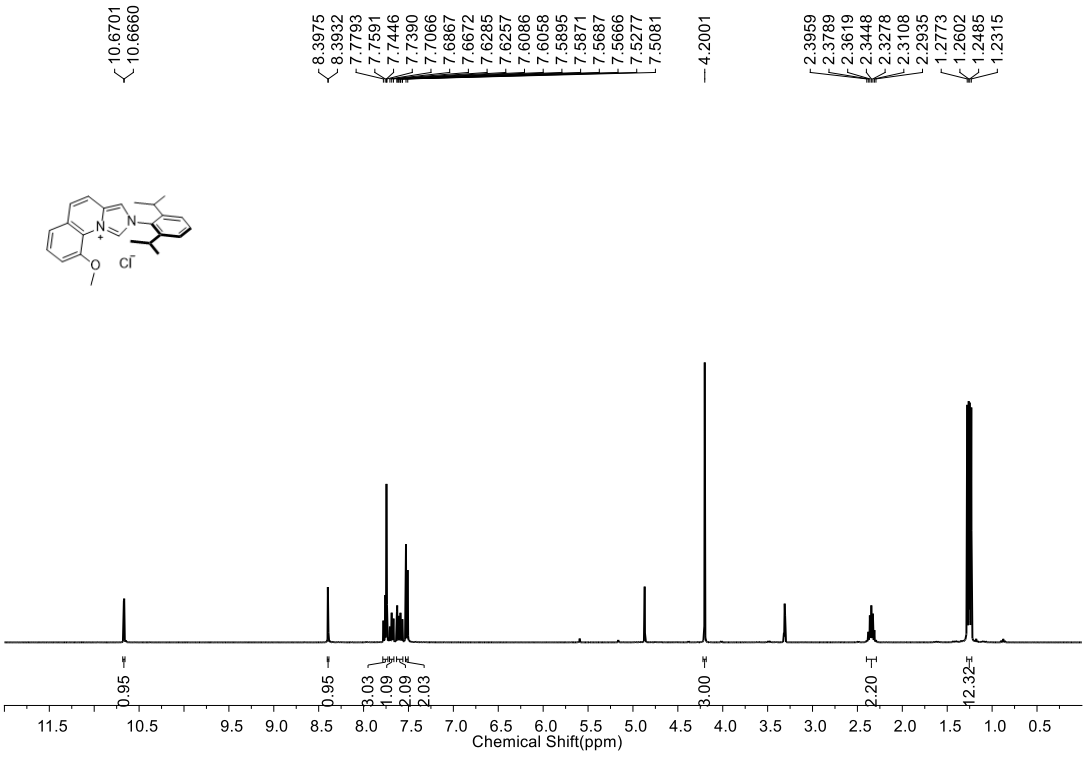

Figure S42 ^{1}H NMR spectrum of **E** in CD_3OD at 25 ℃

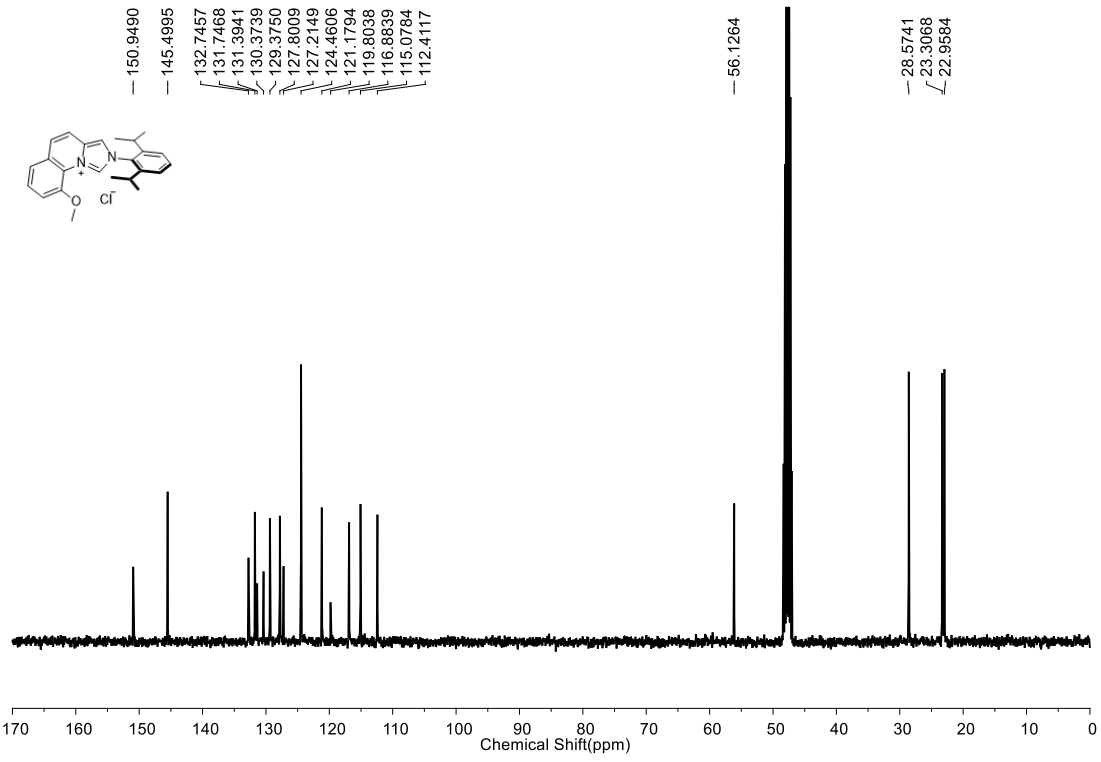

Figure S43 $^{13}C\{^{1}H\}$NMR spectrum of **E** in CD_3OD at 25 ℃

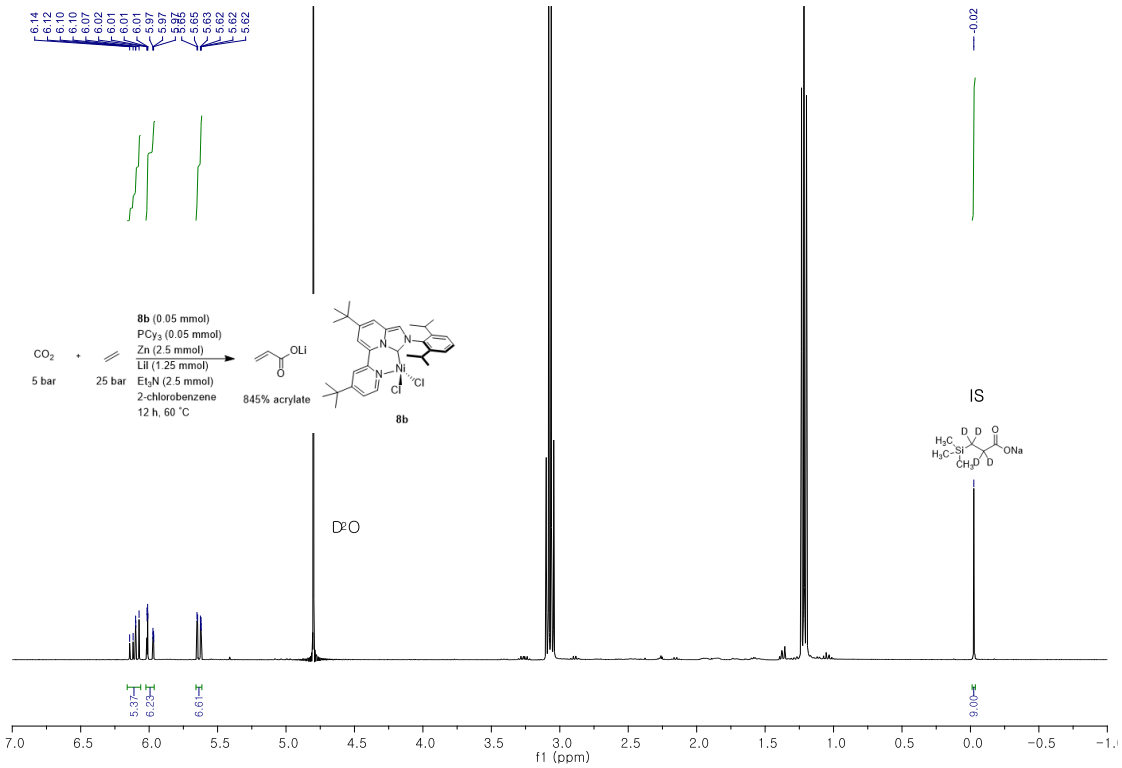

Figure S44 ^{1}H NMR spectrum (in D_2O) of acrylate formation using **8b** (Table 1, entry 10).

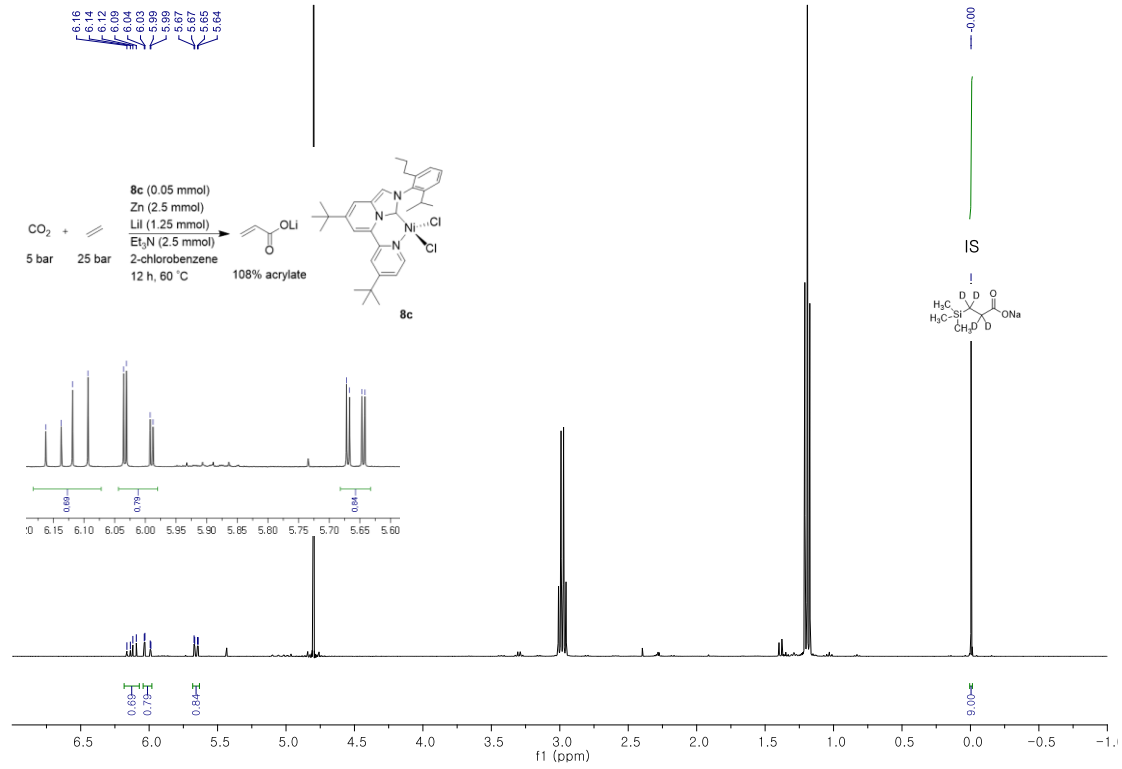

Figure S45 ^{1}H NMR spectrum (in D_2O) of catalytic acrylate formation (Table 1, entry 4).

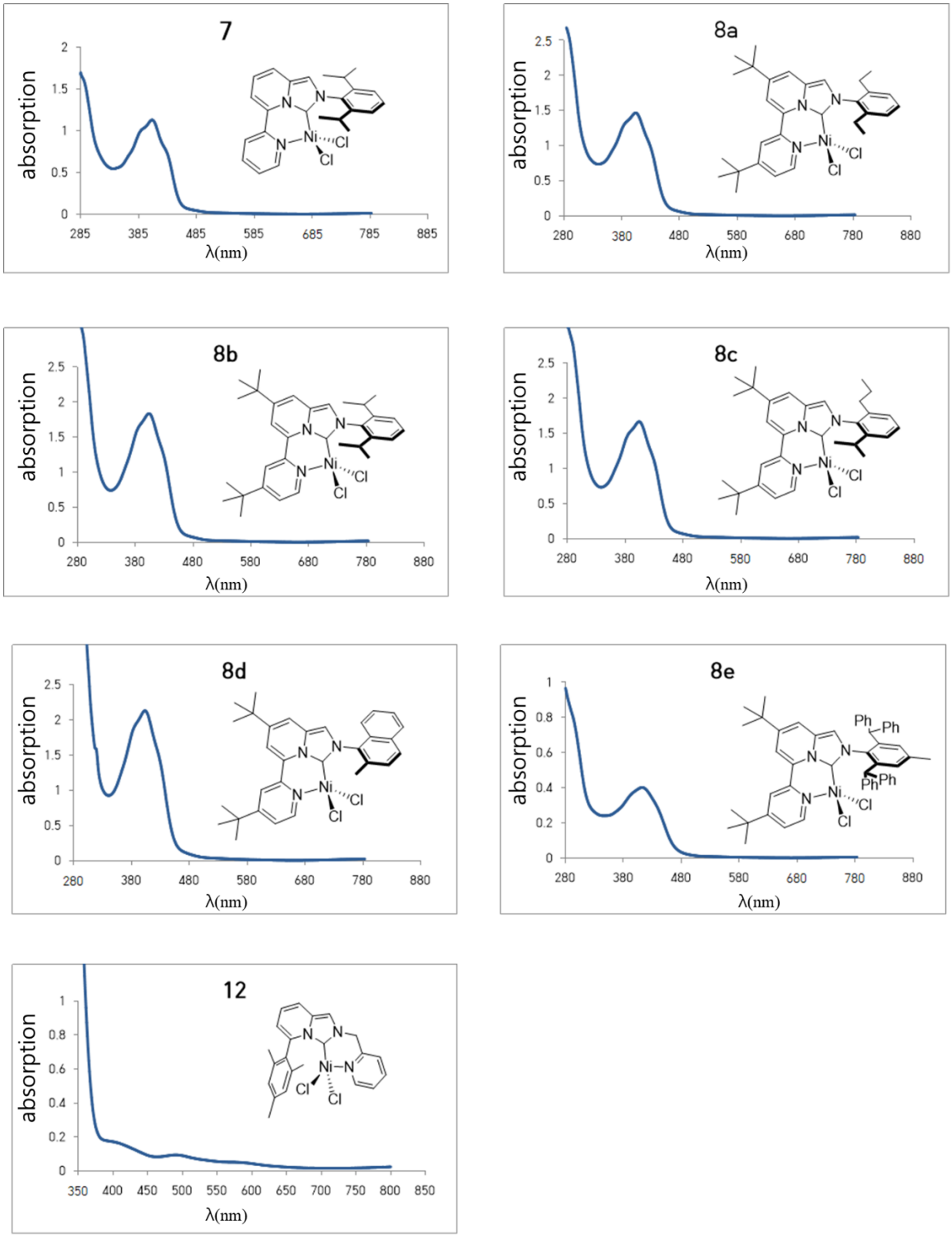

Figure S46 UV-Vis spectroscopy of **7**, **8a-8e**, and **12**

X-ray crystallographic analysis

Reflection data for **3** **4**, **8b** and **12** were collected on a Bruker APEX-II CCD-based diffractometer with graphite-monochromated MoKα radiation (λ = 0.7107 Å). The hemisphere of reflection data were collected as ω scan frames with 0.5°/frame and an exposure time of 10 s/frame. Cell parameters were determined and refined by the SMART program [10]. Data reduction was performed using the SAINT software [11]. The data were corrected for Lorentz and polarization effects. An empirical absorption correction was applied using the SADABS program [12]. The structures of the compounds were solved by direct methods and were refined by following full matrix least-squares methods using the SHELXTL program package with anisotropic thermal parameters for all non-hydrogen atoms [13].

Table S2. Crystallographic data and parameters for **3, 7, 8b** and **12**

	5	**7**	**8b**	**12**
CCDC	1589916	2000471	2000472	2000470
formula	$C_{24}H_{25}AgClN_3$	$C_{24}H_{25}Cl_2N_3Ni$	$C_{32}H_{41}Cl_2N_3Ni$	$C_{22}H_{21}Cl_2N_3Ni$
formula weight	498.79	485.08	597.29	457.03
crystal system	monoclinic	monoclinic	monoclinic	monoclinic
space group	C 1 c 1	P 1 21/n 1	C 1 2/c 1	P 1 21/n 1
a (Å)	14.57975(14)	10.2090(2)	20.5217(6)	9.3714(3)
b (Å)	13.42961(14)	16.6242(4)	17.2804(6)	18.9865(7)
c (Å)	11.4997(1)	13.0759(3)	20.5138(6)	11.6129(4)
α (°)	90	90	90	90
β (°)	99.4746(7)	93.7207(15)	117.966(2)	90.2342(19)
γ (°)	90	90	90	11.6129(4)
V (Å^3)	2220.93(4)	2214.52(9)	6425.2(4)	2066.27(12)
Z	4	4	8	4
ρ_{calc} (g cm^{-3})	1.492	1.455	1.235	1.469
μ (mm^{-1})	1.043	1.134	0.794	1.210
F(000)	1016.0	1008.0	2528.0	944.0
T (K)	100	100	100	100
scan mode	*multi*	*multi*	*multi*	*multi*
hkl range	-19 ≤ h ≤ 19,	-12≤ h ≤ 12,	-20≤ h ≤ 25,	-11≤ h ≤ 11,

	-20 ≤ k ≤17, -16 ≤ l ≤ 16	-20≤ k ≤20, -16≤ l ≤ 15	-21≤ k ≤21, -25≤ l ≤ 25	-20≤ k ≤23, -14≤ l ≤13
measd reflns	9896	6707	9894	9934
unique reflns [R_{int}]	6357 [0.0164]	4230	6248	3940
refined parameters	266	275	353	256
R_1[a] (I > 2σ(I))	0.0186	0.0338	0.0264	0.0950
wR_2[b] all data	0.0446	0.0831	0.0693	0.2579
GOF on F^2	1.059	1.016	1.052	1.136
ρ_{fin} (max/min) (e Å^{-3})	0.266, -0.431	0.390, -0.368	0.416, -0.434	1.754, -1.298

[a] $R1 = \sum||Fo| - |Fc||/\sum|Fo|$. [b] $wR2 = \{[\sum w(Fo^2 - Fc^2)^2]/[\sum w(Fo^2)^2]\}^{1/2}$.

References

1. Knopf, I.; Tofan, D.; Beetstra, D.; Al-Nezari, A.; Al-Bahily, K.; Cummins, C.C. A family of cis-macrocyclic diphosphines: modular, stereoselective synthesis and application in catalytic CO 2/ethylene coupling. *Chemical science* **2017**, *8*, 1463-1468.

2. Hendriksen, C.; Pidko, E.A.; Yang, G.; Schäffner, B.; Vogt, D. Catalytic formation of acrylate from carbon dioxide and ethene. *Chemistry–A European Journal* **2014**, *20*, 12037-12040.

3. Nazari, S.H.; Bourdeau, J.E.; Talley, M.R.; Valdivia-Berroeta, G.A.; Smith, S.J.; Michaelis, D.J. Nickel-Catalyzed Suzuki Cross Couplings with Unprotected Allylic Alcohols Enabled by Bidentate N-Heterocyclic Carbene (NHC)/Phosphine Ligands. *ACS Catalysis* **2018**, *8*, 86-89.

4. Park, D.-A.; Ryu, J.Y.; Lee, J.; Hong, S. Bifunctional N-heterocyclic carbene ligands for Cu-catalyzed direct C–H carboxylation with CO 2. *RSC advances* **2017**, *7*, 52496-52502.

5. Jafarpour, L.; Stevens, E.D.; Nolan, S.P. A sterically demanding nucleophilic carbene: 1, 3-bis (2, 6-diisopropylphenyl) imidazol-2-ylidene). Thermochemistry and catalytic application in olefin metathesis. *Journal of Organometallic Chemistry* **2000**, *606*, 49-54.

6. Tao, W.; Akita, S.; Nakano, R.; Ito, S.; Hoshimoto, Y.; Ogoshi, S.; Nozaki, K. Copolymerisation of ethylene with polar monomers by using palladium catalysts bearing an N-heterocyclic carbene–phosphine oxide bidentate ligand. *Chemical Communications* **2017**, *53*, 2630-2633.

7. Hutt, J.T.; Aron, Z.D. Efficient, single-step access to imidazo [1, 5-a] pyridine N-heterocyclic carbene precursors. *Organic letters* **2011**, *13*, 5256-5259.

8. Pallavicini, P.; Boiocchi, M.; Dacarro, G.; Mangano, C. Enhanced kinetic inertness in the electrochemical interconversion of Cu (I) double helical to Cu (II) monomeric complexes. *New Journal of Chemistry* **2007**, *31*, 927-935.

9. Falivene, L.; Credendino, R.; Poater, A.; Petta, A.; Serra, L.; Oliva, R.; Scarano, V.; Cavallo,

L. SambVca 2. A web tool for analyzing catalytic pockets with topographic steric maps. *Organometallics* **2016**, *35*, 2286-2293.

10. SMART, version 5.0, Data collection software, Bruker AXS, Inc., Madison, WI, 1998.

11. SAINT, version 5.0, Data integration software, Bruker AXS Inc., Madison, WI, 1998.

12. Sheldrick, G. M. SADABS, Program for absorption correction with the Bruker SMART system, Universitat Gottingen, Germany, 1996.

13. Sheldrick, G. M. SHELXL-93: Program for the refinement of crystal structures; Universitat Gottingen: Germany, 1993.